การเปลี่ยนเฟสเชิงโครงสร้างของสแกนเดียมไตรไฮไดรด์ภายใต้ความดันสูง

นายธีรโชติ ภากรโชติ

วิทยานิพนธ์นี้เป็นส่วนหนึ่งของการศึกษาตามหลักสูตรปริญญาวิทยาศาสตรมหาบัณฑิต
สาขาวิชาฟิสิกส์ ภาควิชาฟิสิกส์
คณะวิทยาศาสตร์ จุฬาลงกรณ์มหาวิทยาลัย
ปีการศึกษา 2556

THE STRUCTURAL PHASE TRANSITION OF SCANDIUM TRIHYDRIDE UNDER HIGH PRESSURE

Mr. Teerachote Pakornchote

A Thesis Submitted in Partial Fulfillment of the Requirements
for the Degree of Master of Science Program in Physics
Department of Physics
Faculty of Science
Chulalongkorn University
Academic Year 2013

Thesis Title	THE STRUCTURAL PHASE TRANSITION OF SCANDIUM TRIHYDRIDE UNDER HIGH PRESSURE
By	Mr. Teerachote Pakornchote
Field of Study	Physics
Thesis Advisor	Associate Professor Udomsilp Pinsook, Ph.D.
Thesis Co-advisor	Assistant Professor Thiti Bovornratanaraks, Ph.D.
Thesis Co-advisor	Duck Young Kim, Ph.D.

Accepted by the Faculty of Science, Chulalongkorn University in Partial Fulfillment of the Requirements for the Master's Degree

..... Dean of the Faculty of Science
(Professor Supot Hannongbua, Dr.rer.nat.)

THESIS COMMITTEE

..... Chairman
(Assistant Professor Boonchoat Paosawatyanyong, Ph.D.)

..... Thesis Advisor
(Associate Professor Udomsilp Pinsook, Ph.D.)

..... Thesis Co-advisor
(Assistant Professor Thiti Bovornratanaraks, Ph.D.)

..... Thesis Co-advisor
(Duck Young Kim, Ph.D.)

..... Examiner
(Chatchai Srinitiwarawong, Ph.D.)

..... External Examiner
(Pornjuk Srepusharawoot, Ph.D.)

ธีรโชติ ภากรโชติ : การเปลี่ยนเฟสเชิงโครงสร้างของสแกนเดียมไตรไฮไดรด์ภายใต้ความดันสูง. (STRUCTURAL PHASE TRANSITION OF SCANDIUM TRIHYDRIDE UNDER HIGH PRESSURE) อ.ที่ปรึกษาวิทยานิพนธ์หลัก : รศ.ดร.อุดมศิลป์ ปิ่นสุข, อ.ที่ปรึกษาวิทยานิพนธ์ร่วม : Duck Young Kim, Ph.D., ผศ.ดร.ธิติ บวรรัตนารักษ์, 65 หน้า.

ScH_3 เมื่ออยู่ในใต้ความดันสูงจะเปลี่ยนสถานะเชิงโครงสร้างจากโครงสร้าง hcp เป็นโครงสร้างระหว่างกลาง และเป็นโครงสร้าง fcc ตามลำดับ อย่างไรก็ตามยังไม่มีการค้นพบโครงสร้างที่แท้จริงของโครงสร้างระหว่างกลางของ ScH_3 การคำนวณด้วยทฤษฎีฟังก์ชันนัลของความหนาแน่นให้แนวโน้มเดียวกับการทดลองคือ โครสร้าง hcp จะมีเอนทัลปีต่ำกว่าของโครงสร้าง fcc ที่ความ $0 - 22$ GPa แต่จากการทดลองการด้วยการเลี้ยวเบนรังสีเอ็กซ์ วิธีรามาน และวิธีอินฟราเรด เพื่อตรวจวัดโครงสร้างของ ScH_3 ภายใต้ความดันสูง พบว่าโครงสร้าง fcc เกิดขึ้นที่ความดัน 46 GPa การที่โครงสร้าง hcp ไม่เปลี่ยนเป็นโครงสร้าง fcc ทันทีเมื่ออยู่ภายใต้ความดัน 22 GPa เนื่องมาจากเกิดโครงสร้างระหว่างกลางขึ้นระหว่างสองโครงสร้าง จากการวิเคราะห์พบว่าโครงสร้างระหว่างกลางมีสมมาตรแบบ Cm ซึ่งโครงสร้างระหว่างกลางคือโครงสร้างที่อยู่ระหว่างการเปลี่ยนรูปแบบของระนาบสแกนเดียมจากแบบ ABABAB ไปสู่แบบ ABCABC ซึ่งเมื่อนำผลของระยะระหว่างระนาบของโครงสร้างระหว่างกลางที่ได้จากการคำนวณไปเปรียบเทียบกับผลที่ได้จากการทดลองแล้วพบว่ามีความสอดคล้องกัน

ภาควิชา ฟิสิกส์ ..... ลายมือชื่อนิสิต .....

สาขาวิชา ฟิสิกส์ ..... ลายมือชื่อ อ.ที่ปรึกษาวิทยานิพนธ์หลัก .....

ปีการศึกษา 2556 ..... ลายมือชื่อ อ.ที่ปรึกษาวิทยานิพนธ์ร่วม .....

ลายมือชื่อ อ.ที่ปรึกษาวิทยานิพนธ์ร่วม .....

5471992023 : MAJOR PHYSICS
KEYWORDS: SCANDIUM TRIHYDRIDE/ PHASE TRANSITION/ DENSITY FUNCTIONAL THEORY

TEERACHOTE PAKORNCHOTE : THE STRUCTURAL PHASE TRANSITION OF SCANDIUM TRIHYDRIDE UNDER HIGH PRESSURE. ADVISOR : ASSOC. PROF. UDOMSILP PINSOOK, Ph.D., CO-ADVISOR : ASST. PROF. THITI BOVORNRATANARAKS, Ph.D., DUCK YOUNG KIM, Ph.D., 65 pp.

The ScH_3 transforms from hcp phase to intermediate phase to fcc phase under high pressure, however, the exact structure of the intermediate phase was not realized for the exact structure. The phase transition of ScH_3 had been investigated by the X-ray diffraction, Raman and infrared experiments. The theoretical calculation using density functional theory is consistent with as the experiments that the hcp phase has the enthalpy lower than the fcc phase at $0 - 22$ GPa. The experiment showed that the fcc phase occurs at 46 GPa. The transition pressure obtained in the theoretical study that is lower than that of the experiment can be explained by the sluggishness of the intermediate phase. The structural analysis showed that the intermediate phase has the Cm symmetry. The intermediate phase is among the changing pattern of scandium planes from ABABAB to ABCABC stacking sequence. The d-spacing of the intermediate phase is in good agreement with experiment.

Department:.....Physics.....Student's Signature .....

Field of Study:.....Physics.....Advisor's Signature .....

Academic Year:.....2013.....Co-advisor's Signature .....

Co-advisor's Signature .....

ACKNOWLEDGEMENTS

I appreciate to work at the ECPRL (Extreme condition physics research laboratory) group. The research in this field has to have diverse knowledge, however, the memberships of ECPRL group always kindly give an advice to pass the difficult learning. We have many discussions together that improve our knowledge and research skill. I would like to thanks all of the membership that help me to overcome many obstacles among the research, until I finish my thesis. I am very grateful to Assoc. Prof. Dr. Udomsilp Pinsook that always kindly gives me suggestions, and also points the weak point and the direction of my research. I am thankful for Asst. Prof. Dr. Thiti Bovornranaraks and Dr. Duck Young Kim who are my co-advisors that suggest many good advices and I also would like to acknowledge Asst. Prof. Dr. Nakorn Phaisangittisakul for useful discussions. Moreover, I would like to thankful the examination committees; Asst. Prof. Dr. Boonchoat Paosawatyanyong, Dr. Chatchai Srinitiwarawong and Dr. Pornjuk Srepusharawoot. I am grateful to Dr. Ayako Ohmura for very useful experimental results. This thesis has been partially supported by National Research Council of Thailand (NRCT) and Thailand center of Excellence in Physics (ThEP). Computing facilities are supported by Chulalongkorn University Centenary Academic Development Project (CU56-FW10) and A1B1 funding from Faculty of Science, Chulalongkorn University. T.B. acknowledge TRF contract number RSA5580014. Computing facilities have been partially provided by the Ratchadaphiseksomphot Endowment Fund of Chulalongkorn University (RES560530180-AM) and the Special Task Force for Activating Research (STAR), Ratchadaphiseksomphot Endowment Fund, Chulalongkorn University through the Energy Materials Physics Research Group.

CONTENTS

page

page

LIST OF TABLES

Table **page**

LIST OF FIGURES

Figure **page**

Chapter I

INTRODUCTION

Scandium is a trivalent rare-earth element which is in the same row as yttrium and lanthanum. Yttrium and lanthanum hydride can be used as a switchable mirror [1]. Their compositions can be switched between dihydride which is a metal phase and trihydride which is a semiconductor phase. The metal phase is an excellence metal and shiny while the semiconductor phase is transparent in the visible frequency range. Indeed, all of the trivalent rare-earth hydride were suggested to have this switchable optical property, also. Moreover, from theoretical studies, the trivalent rare-earth trihydride have superconductivity under high pressure [2]. The properties i.e. physical property, electrical property and optical property are affected by different phases of structures. In this thesis, we considered the structures of scandium trihydride under pressure which will be very useful for the study of its properties in the future.

The X-ray diffraction (XRD) experiment of scandium hydride was done by A. Ohmura et al [3]. The fragment of scandium which has diameter 60 μm and thickness 15 μm was hydrogenated under high pressure and at room temperature in the diamond anvil cell (DAC). The ScH_x occurred at 0.43 GPa with x $\sim$ 0.43 and it has a hexagonal pattern. The concentration of hydrogen was increase as the pressure increases. When the pressure reached 4.1 GPa, the peak of XRD pattern* indicated the ScH_2 appeared and is a fcc phase. The ScH_3 formed at 5.3 GPa and is a hcp phase while the ScH_2 remained. The volume fraction of ScH_2 reduced from 68 % at 5.3 GPa to 25 % at 20.9 GPa. Actually, the XRD cannot detect the hydrogen atoms, so they separated the ScH_2 and ScH_3 by extrapolating the data and compared the lattice parameters to that of the neutron diffraction [4] at 1 atm. Even the ScH_3 and the other REH_3 (RE = rare earth) are the hcp pattern by metal planes but the neutron diffraction showed that the space group of $ScH_{2.90}$ differs from of the others which are $P\bar{3}c1$. The ScH_2 powder was pressurized with hydrogen at 1 GPa and 250 $^\circ C$ for 24 h to do the hydrogenation.

*see in Appendix A.

The sample was cooled at 150 K and then was released from high pressure cell. The 1.2 g of $ScH_{2.90}$ powder was done the neutron diffraction experiment at 97 K. The neutron diffraction pattern could not fit with the $P\bar{3}c1$ pattern or even the $P6_3/mmc$ pattern. The metal planes are the same pattern of cause which is the hcp, however, the hydrogen atoms arrange in a difference pattern. The atomic positions are showed in Table 1.1 with the $P6_3/mmc$ symmetry structure. There are three hydrogen atoms; two of them occupy at tetrahedral sites[†] (T site) which refer to H_t atoms and the another one occupies on metal plane (M site) which refers to H_m atom. Nevertheless, the neutron diffraction pattern showed no sign of long-range hydrogen ordering. The H_t and H_m atoms of $ScH_{2.90}$ were displaced from the ideal T site and M site, respectively. The $P6_3/mmc$ symmetry structure gives that four H_m atoms form two dumbbells along the c axis but the site occupancies (ω) is 0.48. Therefore, there are only half of them can be occupied on this site and the distributions of H_m atoms are random over this sites. Moreover, the thermal factors of hydrogen atoms in Table 1.1 are very large that cause the hydrogen atoms diffuse away from their equilibrium positions.

Table 1.1: The atomic positions of hcp phase are calculated by applying the $P6_3/mmc$ symmetry structure to ScH_3 when B is the thermal factor and ω is the site occupancy. [4]

Atom	Site	x	y	z	B (Å^2)	ω
Sc	$2c$	1/3	2/3	1/4	0.46	1.00
H_t	$4f$	1/3	2/3	-0.088	2.40	0.97
H_m	$4e$	0	0	0.210	1.50	0.48

The c/a of REH_3 are reduced obviously while they were compressed under high pressure. In contrast to the c/a of ScH_3 that remain about 1.8 for a wide range of pressure $4-30$ GPa. The peaks of XRD pattern of the hcp started to lose their intensity and of the fcc started to increase their intensity at about 30 GPa. The occurrence of the fcc was complete at about 46 GPa until the XRD experiment was end at 54.7 GPa. The phase between the hcp and the fcc is the intermediate phase. The d-spacing of the intermediate phase shows the connection that which planes of the hcp transform to which planes of the fcc (see Fig 1.1a). The $(101)_h$ plane was split into two planes at the intermediate phase and then transform to

[†]see in Appendix B.

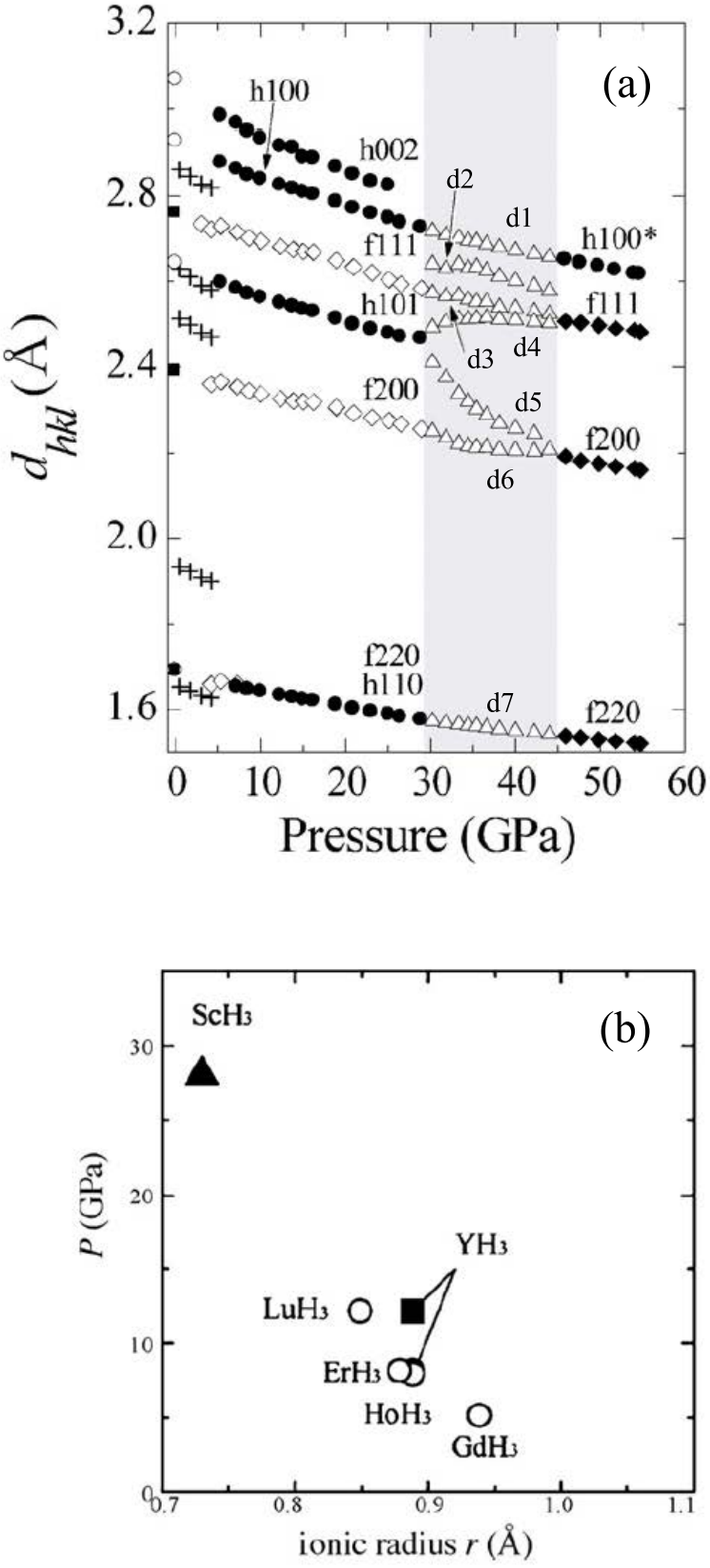

Figure 1.1: (a) The d-spacing of several planes of ScH_3 under high pressure. The planes of hcp, intermediate and fcc phases are different, so they are the virtue for structural analysis. (b) The ionic radii of REH_3 is shown that the relationship to the transition pressure is inversely proportional. [3]

the $(111)_f$ and $(200)_f$ planes, respectively. The $(110)_h$ plane decreased smoothly through the intermediate phase and then transform to the $(220)_f$ continuously. The hcp-intermediate phase transformation pressures of the REH_3 are inversely proportional the ionic radii (see Fig 1.1b). The ScH_3 has the ionic radii 0.73 Å, so that it has the same tendency of the relation between transformation pressure and the ionic radii of the REH_3.

The Raman experiment used the sample of 5 μm thin which is thinner than that of the XRD experiment, so T. Kume et al [6] believed that the percent of ScH_2 is lesser. It showed that there is the Raman-active at O_v mode under pressure < 25 GPa which is active when there are no hydrogen atoms at octahedral sites (O sites) and is inactive when there are hydrogen atoms at O sites. The result is accordance to the neutron diffraction result. The H_t mode cannot be measured because it has the frequency around 1,200 cm^{-1} but it was concealed by the strong diamond signal around 1,330 cm^{-1}. The Sc mode is discontinuously shifted at $>$ 25 GPa imply that the stacking sequence of the metal planes changed. On the other hand, the infared (IR) experiment found that the hcp-intermediate phase transition occurred at 28 GPa, so from the three experiments, XRD, Raman and IR, it can be concluded that the intermediate phase coexists with the hcp phase at $25-30$ GPa. The Raman peak of O_v disappeared at the intermediate phase, so that the hydrogen atoms moved to the O site. Nevertheless, there are not every of them move to the O site. The extremely broad band possibly indicated that the hydrogen atoms have some distribution around the O site and may correspond to the wave modulation which is larger than, or is incommensurately matched with, the lattice parameters. The Grüneisen parameters (γ) were calculated for the hydrogen modes at the O site and T site. The γ show that the bonding between Sc and H_o is covalent and between Sc and H_t is ionic. The first two Raman peaks of ScH_3 and YH_3 at the intermediate phase are similar. The structure of the intermediate phase YH_3 was studied by matching the experimental XRD pattern to the theoretical XRD pattern, and so it has the long-period stacking sequence of metal planes that is the hcp and fcc mixed up together [5]. However, we will suggest the alternative intermediate phase of ScH_3 by analysis the d-spacing in Chapter IV.

The phase transition of ScH_3 was studied by using density functional theory (DFT). The DFT and the other involved theory, i.e., crystal structure, phase stability and technique of calculation, will be explained in Chapter II. The method of calculation and the details of the structure will be shown in Chapter III. The

results of the study, i.e., the phase transition and the details of the intermediate phase, will be discussed in Chapter IV. And last, the conclusion will be concluded in Chapter V.

Chapter II

THEORY

The research in condense matter or materials science reaches the era of the integrated knowledge that we have to mix many subjects together to find what we are finding. This research is about the transformation of structures. The crystallography plays the important role to analyze the crystal structures of interesting materials. The density functional theory (DFT) can calculate the energy and the properties of those structures. The phase transition theory is based on the equation pf states and the lowest due energy state. Let us begin with the crystal structure.

2.1 Crystal structure

The atoms in solid are arranged in an orderly fashion. The atom and its neighbors form a periodic pattern. The copies of pattern are lined up infinitely. Therefore, the microscopic structure of solid is order and periodicity. It is the so-called crystal structure. The macroscopic structure of solid may contian some defects and the properties change slightly.

2.1.1 Lattice

Lattice is where there are points that put on the empty space and spread uniformly in three dimension (3D) (see Fig 2.1a). Even we stand on any point and look around, they are the same. We can move from one point to another point by the translation vector which connects any two points, and the environment remains unchange. If the atoms are put in each lattice point, it becomes the crystal. However, the atom can place on a basis which is related to the lattice point by an extra coordinate (x, y, z) in (3D), e.g., the basis of the atom placed at the lattice point is (0,0,0) (see Fig 2.1b). The lattice point with the basis is repeated to consist of the lattice and becomes crystal (see Fig 2.1c).

2.1.2 Unit cell

The lines connect a point to a nearest point in lattice joint together as a block. Each block can be arranged without empty space. This block defines a unit cell. It can contain atoms inside which may be more than one atom. If there is one atom inside unit cell which repeat itself in space, it is a primitive cell. Some unit cells that contain more than one atom can be reduced into a primitive cell. If a primitive cell exists, it will help improve computing time consumption.

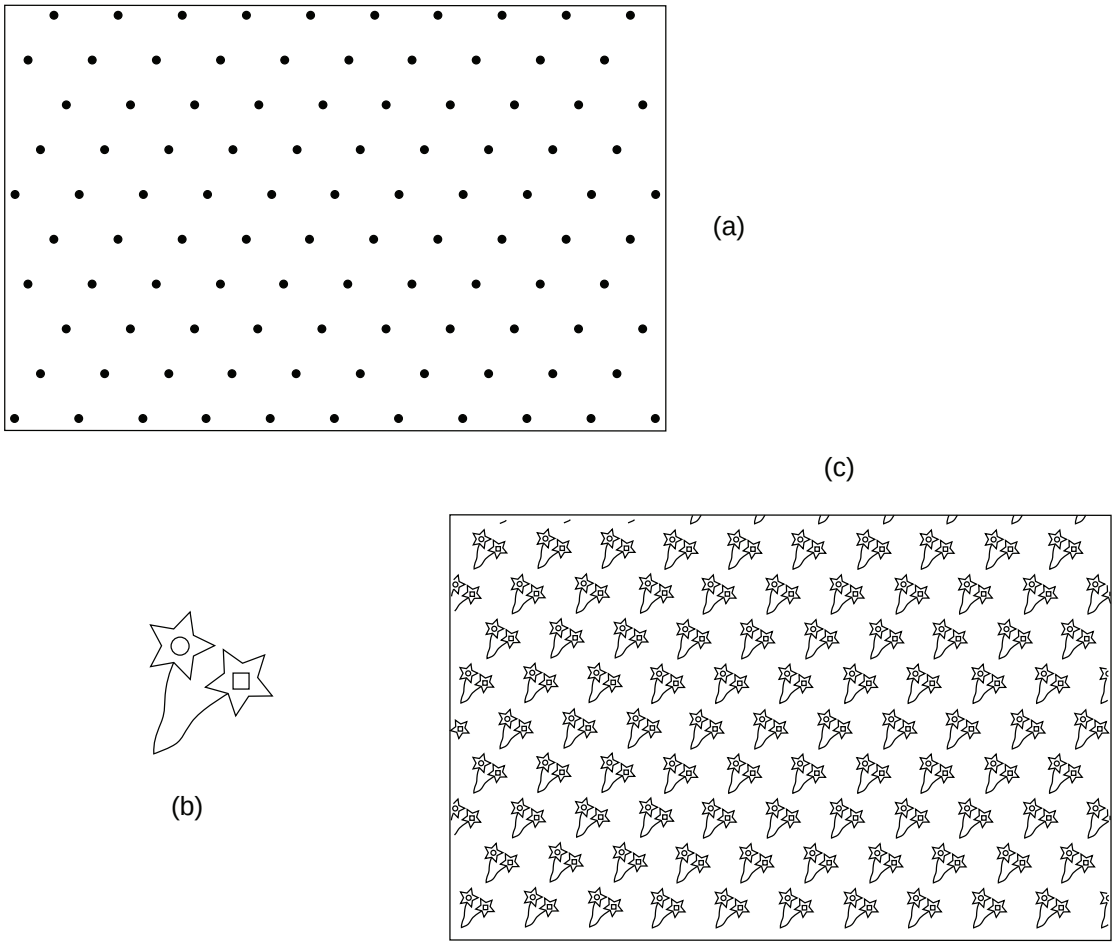

Figure 2.1: (a) The points spread uniformly to form the net in 2D and the lattice in 3D. (b) The stars germinate from the origin. (c) The crystal consists of the lattice and the basis.

2.1.3 Bravias lattice

Bravias lattice has 14 forms of unit cells which are based on 7 lattice systems in 3D. This is the base system. There are no lattice forms beyond the Bravias lattice and if there are other forms, they can be reformed into Bravias lattice.

2.1.4 Space groups

Space groups are the symmetry applied in Bravias lattice with various formations, i.e. rotation axis, inversion, mirror plane, translation and glide axis. There are 230 space groups in 3D. This work regards the hcp and fcc as the main structure which have space groups $Fm\bar{3}m$ and $P6_3/mmc$, respectively.

2.1.5 Plane, direction and d-spacing

A Plane can be defined as a flat plate that traverses through a set of atoms. It is specified by three inverse numbers that the plane intersects to principal axes. This numbers are called Miller index which is written as (hkl). If there are planes that traverse the same set of atoms, they can be grouped together and written as hkl. Planes for each kind of a lattice system are difference, so the plane is labeled to distinguish when it is referred to. In this work, we use subscript h, for hcp, f for fcc and Cm for Cm groups. The direction points from the origin to perpendicular to the plane, can be written as

$$\mathbf{r} = u\mathbf{a} + v\mathbf{b} + w\mathbf{c}. \tag{2.1}$$

It can be written in shorthand as $[uvw]$ to tell the direction. The d-spacing is the distance between two parallel planes. It is advantageous in XRD experiment to define the structure using Braggs law,

$$n\lambda = 2d_{hkl}\sin\theta, \tag{2.2}$$

and also using the equation of d-spacing in Table 2.1.

2.1.6 Close packed structure

A close packed structure is the most compact structure of identical spheres. One sphere is placed at the center has be surrounded by 6 spheres most in two dimensions (2D) called hexagonal form. The 6 surrounded spheres in the same plane packed together and there exists 6 voids which is the hollows among the spheres (see Fig 2.2). The voids can be filled by above and/or below 2D close packed layer compactly, even though a layer can fill only half of the voids. Therefore, if we regard in 3D, there are many combinations of close packed layers by the patterns of stacking layers.

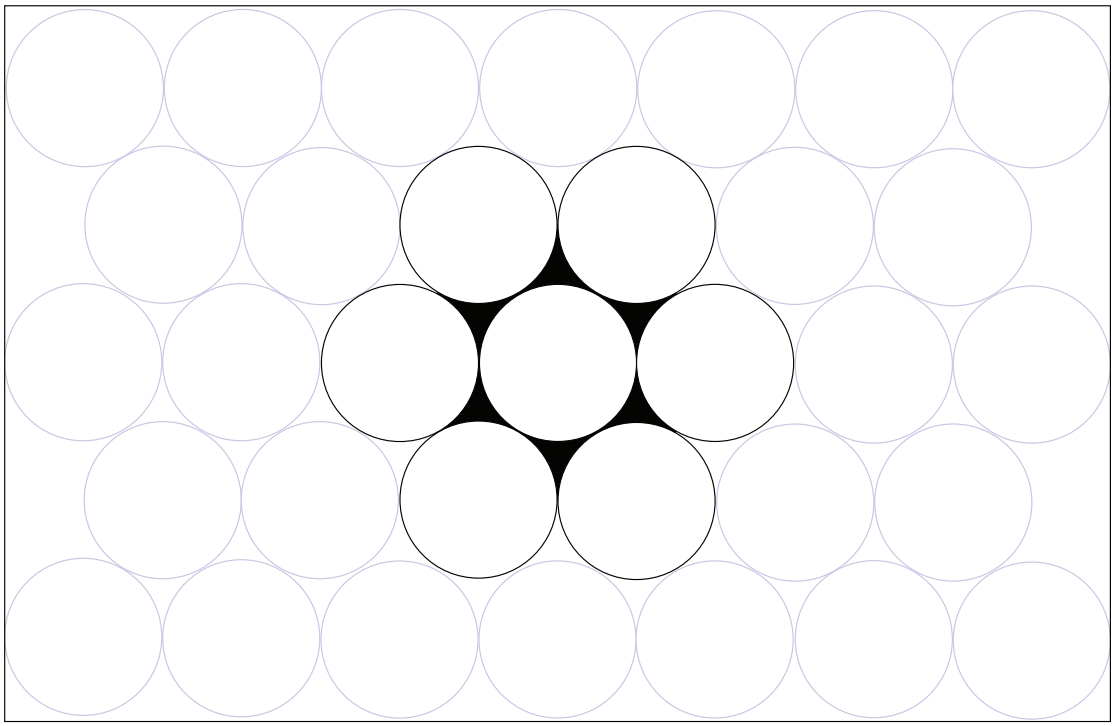

Figure 2.2: The spheres form the closest pack. The black areas are the voids that the spheres cannot fill.

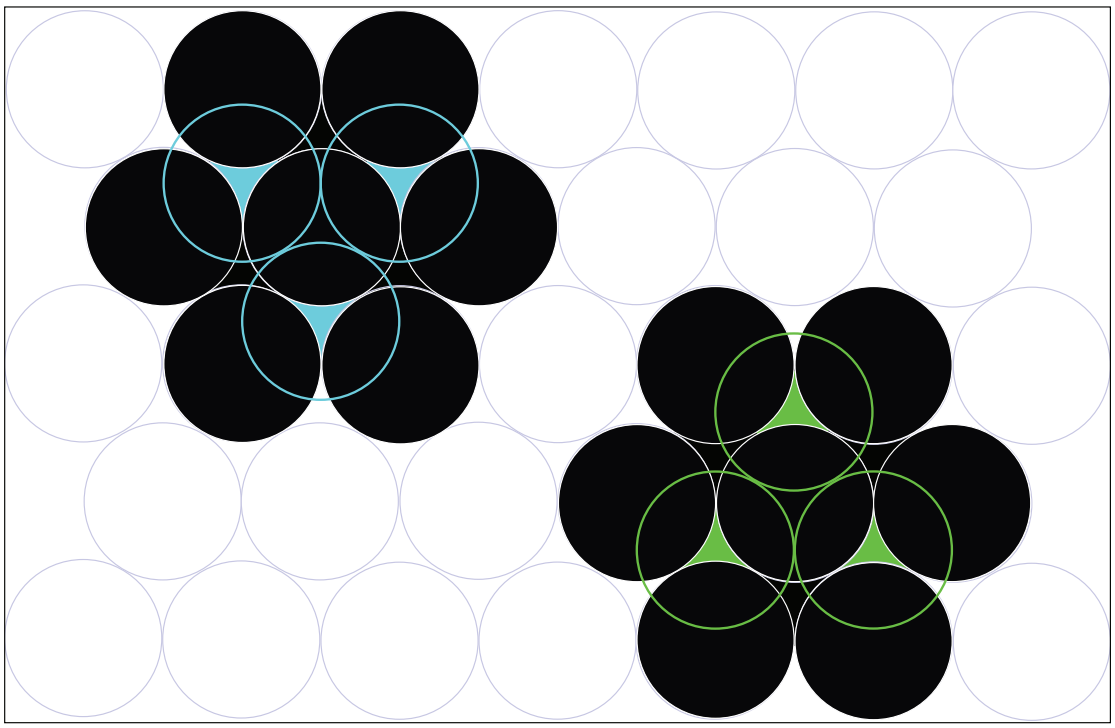

Figure 2.3: The hollow circles represent the spheres that place above the black spheres. They can pile up only half of the voids of the below layer, so there are another half that can be filled.

Table 2.1: The expressions of the d_{hkl} value of the various crystal systems are showed in the inverse square form.

System	$1/d_{hkl}^2$
Cubic	$(h^2+k^2+l^2)/a^2$
Tetragonal	$\frac{h^2+k^2}{a^2}+\frac{l^2}{c^2}$
Orthorhombic	$\frac{h^2}{a^2}+\frac{k^2}{b^2}+\frac{l^2}{c^2}$
Hexagonal	$\frac{4}{3a^2}(h^2+k^2+hk)+\frac{l^2}{c^2}$
Trigonal	$\frac{1}{a^2}\left(\frac{(h^2+k^2+l^2)\sin^2\alpha+2(hk+hl+kl)(\cos^2\alpha-\cos\alpha)}{1+2\cos^3\alpha-3\cos^2\alpha}\right)$
Monoclinic	$\frac{h^2}{a^2\sin^2\beta}+\frac{k^2}{b^2}+\frac{l^2}{c^2\sin^2\beta}-\frac{2hl\cos\beta}{ac\sin^2\beta}$
Triclinic	$(1-\cos^2\alpha-\cos^2\beta-\cos^2\gamma+2\cos\alpha\cos\beta\cos\gamma)^{-1}$ $\times\left(\frac{h^2}{a^2}\sin^2\alpha+\frac{k^2}{b^2}\sin^2\beta+\frac{l^2}{c^2}\sin^2\gamma+\frac{2kl}{bc}(\cos\beta\cos\gamma-\cos\alpha)\right.$ $\left.+\frac{2lh}{ca}(\cos\gamma\cos\alpha-\cos\beta)+\frac{2hk}{ab}(\cos\alpha\cos\beta-\cos\gamma)\right)$

The easiest structure is called the simple hexagonal (sh) that the next layers do not fill any voids or we can say that there are no stacking layers for sh. Because all layers are placed on the same position, so it has a pattern, AAAA$\cdots$ which A means the starting layer and its equivalent layers. The most well-known patterns of stacking layers are ABABAB and ABCABC which are so-called hexagonal close-packed (hcp) and face-centered cubic (fcc), respectively. B means that the above layer fills 3 of 6 voids from the first layer. C means that the above layer fills different 3 voids after B (see Fig 2.3). Even they are close packed structure, but the hcp is in the hexagonal system and the fcc is in cubic system. As they are different by stacking layers, they can transform continuously to each other by sliding layer. The sphere will be moved from a void to another nearest void with a shortest distance to change the pattern. The sphere is placed at the void which is the center of the equilateral triangle. The laterals of the equilateral triangle are a lattice parameter of a hexagonal unit cell (a). We have known that the distance from the vertex to the center is the two-third of the altitude. The magnitude of

the altitude is

$$h = \frac{\sqrt{3}}{2}a. \tag{2.3}$$

Fig 2.4 shows that the nearest voids are in the next articulate equilateral triangle. The distance between two nearest voids, d, is two-third of the altitude, however, if we regard the two equilateral triangle as a rhomboid, it is the one-third of a long diagonal of the rhomboid. The long diagonal of the rhomboid is twice of the altitude, so

$$d = \frac{\sqrt{3}}{3}a. \tag{2.4}$$

It is advantageous to build the intermediate structure in Chapter 3 and the mechanism of the transformation between the hcp and fcc patterns will be described in Chapter 4.

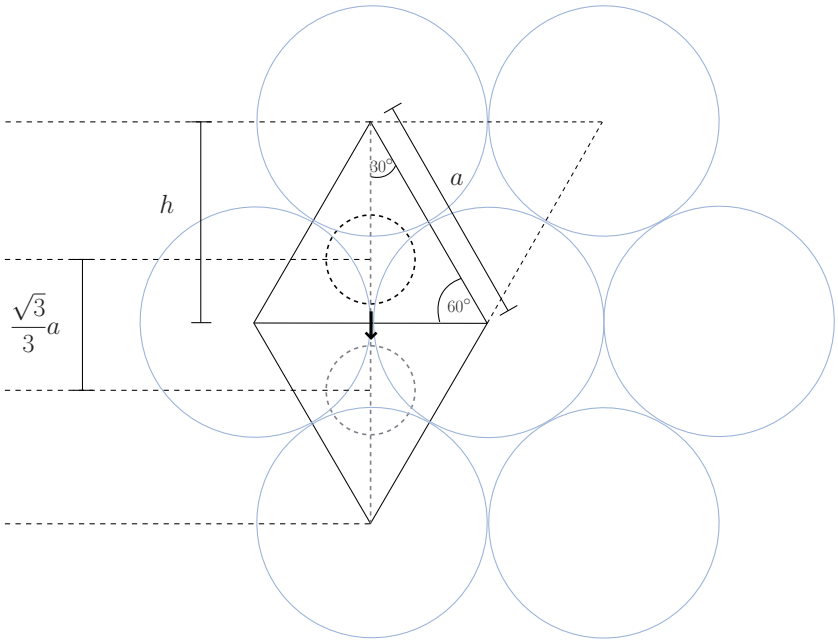

Figure 2.4: The geometry of the close packed structure. The black arrow points the direction that the sphere can move to the other void with a shortest distance.

2.2 Phase stability

In thermodynamics, the irreversible transformation of the system from the initial equilibrium indicates to the increasing of entropy

$$\delta S \geq 0 \quad \text{or} \quad S_f \geq S_i. \tag{2.5}$$

The Eq 2.5 shows that the final state entropy, S_f, is higher than the initial state entropy, S_i. If we assume that the system is changed infinitesimally, the system will evolve until the entropy reaches the maximum at the final equilibrium

$$S = S_{max}. \tag{2.6}$$

In solid, a system is always contacted with thermal and pressure reservoir. It can have initial the temperature, T_0, and pressure, P_0, which differ from the reservoir, and then they will be evolved until the system reaches equilibrium. This evolution makes the higher entropy

$$\delta S_{sys} + \delta S_{res} \geq 0, \tag{2.7}$$

The entropy of the reservoir, S_{res}, changes because it transfers heat into the system but the temperature is unchanged

$$\delta S_{res} = -\frac{Q}{T_0}. \tag{2.8}$$

Putting the Eq 2.7 in the Eq 2.8

$$Q - T_0 \delta S \leq 0. \tag{2.9}$$

The first law of thermodynamics is stated with constant pressure

$$\delta U = Q - P_0 \delta V, \tag{2.10}$$

where U is the internal energy which can be computed by DFT and V is the volume. The Eq 2.9 is applied to the Eq 2.10, so

$$\delta U + P_0 \delta V - T_0 \delta S \leq 0, \tag{2.11}$$

$$\delta(U + PV - TS) = 0, \tag{2.12}$$

$$\delta \mathcal{G} \leq 0. \tag{2.13}$$

In our calculation, however, there is no temperature applied to the system, so it is surrounded by the 0 K environment. The Gibbs free energy ($\mathcal{G}$) is reduced to the enthalpy free energy ($\mathcal{H}$)

$$\delta \mathcal{H} = \delta U + P_0 \delta V, \tag{2.14}$$

$$\delta \mathcal{H} \leq 0. \tag{2.15}$$

The Eq 2.15 is the condition that the system which is contacted with 0 K, and pressure reservoir will evolve until the enthalpy reaches the minimum

$$\mathcal{H} = \mathcal{H}_{min}. \tag{2.16}$$

Therefore, the phases which have the lowest enthalpy is the most preferable for the system. We apply Eq 2.16 to analyze the phase transition.

2.3 Density functional theory

The condensed matter system consists of enormous electrons that distribute around their nuclei. The number of electrons and nuclei are difference in each system. The nuclei can be bound together by some kinds of bond, i.e., metallic bond, covalent bond, and ionic bond. Each kind of bond gives different physical property, optical property and other properties. The valence electrons play the important role in bonding. Therefore, the density functional theory (DFT) describes the electrons and the density refers to electron density. The behavior of the electrons can be solved by the quantum mechanics, then we start from considering the Schrödingers equation,

$$\hat{H}\Psi(\mathbf{r}_1,\ldots,\mathbf{r}_{N_e},\mathbf{R}_1,\ldots,\mathbf{R}_{N_n}) = E\Psi(\mathbf{r}_1,\ldots,\mathbf{r}_{N_e},\mathbf{R}_1,\ldots,\mathbf{R}_{N_n}), \tag{2.17}$$

when

$$\begin{aligned}\hat{H} = &-\sum_i \frac{1}{2}\nabla_{r_i}^2 - \sum_I \frac{1}{2M_I}\nabla_{R_I}^2 \\ &+ \frac{1}{2}\sum_{i\neq j}\frac{e^2}{|\mathbf{r}_i-\mathbf{r}_j|} + \frac{1}{2}\sum_{I\neq J}\frac{Z_I Z_J e^2}{|\mathbf{R}_I-\mathbf{R}_J|} - \sum_{i,I}\frac{Z_I e^2}{|\mathbf{r}_i-\mathbf{R}_I|}.\end{aligned} \tag{2.18}$$

The indices and mass which are small letters and capital letters are of electrons and nuclei, respectively. The N_e is an amount of electron and N_n is an amount of nuclei. The first and second terms on the right hand side (RHS) in Eq 2.3 are the kinetic energy of electron and nuclei, respectively. The last three terms on RHS in Eq 2.3 are Coulomb interactions between particles which are electron-electron, electron-nuclei and nuclei-nuclei, respectively. Even the equation of system is easy to write but its solution is very difficult and complicated to solve. Because the wave function is depends on $3N_e + 3N_n$ variables. Therefore, it needs to be approximated to make an easier problem. There are two parts that can be approximated, i.e., the Hamiltonian and the wave function. The dynamic of the electrons is enormous higher than of the nuclei, so the electrons see the movement of the nuclei likes stationary. The coordinates of electrons can be separated out of the coordinates of nuclei in the wave function,

$$\Psi(\mathbf{r}_1,\ldots,\mathbf{r}_{N_e},\mathbf{R}_1,\ldots,\mathbf{R}_{N_n}) = \Psi(\mathbf{r}_1,\ldots,\mathbf{r}_{N_e})\Psi(\mathbf{R}_1,\ldots,\mathbf{R}_{N_n}). \tag{2.19}$$

The nucleus part in Hamiltonian can be set as constants when the Hamiltonian operates on electron wave function, so the degree of fredom is reduced to N_e. It is called Born-Oppenheimer approximation

$$\hat{H}\Psi(\mathbf{r_1},\ldots,\mathbf{r_{N_e}}) = E\Psi(\mathbf{r}_1,\ldots,\mathbf{r_{N_e}}), \tag{2.20}$$

when

$$\hat{H} = -\sum_i \frac{1}{2}\nabla_{r_i}^2 + \sum_i v(\mathbf{r}_i) + \frac{1}{2}\sum_{i\neq j}\frac{e^2}{|\mathbf{r}_i - \mathbf{r}_j|}. \tag{2.21}$$

The $v(\mathbf{r}_i)$ is the nuclei-electron interaction. It is a background potential that has the electron moving around with electron-electron interaction. In general case, $v(\mathbf{r}_i)$ is an external potential that includes external forces in the background.

2.3.1 Hartree-Fock approximation

Although, the number of variables in the wave function is reduced to $3N_e$ but it is still too many. Hartree proposed that the electron wave function can be purely separated by multiplication. The electron wave function is reduced from an electron wave equation with $3N_e$ variables to single $3N_e$ electron wave equations with $\mathbf{r}_i$ variable each. But the electron is the fermion, so it must be obey the Pauli's exclusion principle,

$$\Psi(\mathbf{r}_1, \mathbf{r}_1) = 0, \tag{2.22}$$

which two electron cannot be filled in the same state, and electron wave function must be antisymmetric,

$$\Psi(\mathbf{r}_1, \mathbf{r}_2) = -\Psi(\mathbf{r}_2, \mathbf{r}_1). \tag{2.23}$$

Later, Slater proposed the electron wave function in the form of determinant that contains those information,

$$\Psi = \frac{1}{\sqrt{N!}}\begin{vmatrix} \psi_1(\mathbf{r}_1) & \psi_2(\mathbf{r}_1) & \cdots & \psi_N(\mathbf{r}_1) \\ \psi_1(\mathbf{r}_2) & \psi_2(\mathbf{r}_2) & \cdots & \psi_N(\mathbf{r}_2) \\ \vdots & \vdots & \ddots & \vdots \\ \psi_1(\mathbf{r}_N) & \psi_2(\mathbf{r}_N) & \cdots & \psi_N(\mathbf{r}_N) \end{vmatrix}, \tag{2.24}$$

$$= \frac{1}{\sqrt{N!}} det[\psi_1(\mathbf{r}_1)\psi_2(\mathbf{r}_2)\cdots\psi_N(\mathbf{r}_N)]. \tag{2.25}$$

Now, we set N as the number of electron. Even though, the Hartree-Fock energy still has the energy difference from the true energy. The difference energy is a correlation energy

$$E_{corr}^{HF} = E - E_{HF}, \tag{2.26}$$

which can be calculated by, e.g., the Kohn-Sham method.

2.3.2 Hohenberg-Kohn theorem

Thomas and Fermi were the pioneers who played with the electron density to explain a homogenous electron gas. Hohenberg and Kohn picked the idea up and

then use it to explain an inhomogenous electron gas which is more precise for the electron in the condensed matter [7]. They derived two theorems that support DFT calculation so well. First, we have to rewrite the Hamiltonian in the form of a density functional as

$$E[\rho] = T_s[\rho] + V_{ext}[\rho] + U[\rho]. \tag{2.27}$$

when

$$T_s[\rho] = \int -\frac{1}{2}\nabla^2_{\mathbf{r}}\rho_1(\mathbf{r}', \mathbf{r})_{\mathbf{r}'=\mathbf{r}} d\mathbf{r}, \tag{2.28}$$

$$V_{ext}[\rho] = \int v(\mathbf{r})\rho(\mathbf{r})d\mathbf{r}, \tag{2.29}$$

$$U[\rho] = \iint \frac{1}{\mathbf{r}_2 - \mathbf{r}_1}\rho_2(\mathbf{r}_1, \mathbf{r}_2)d\mathbf{r}_1 d\mathbf{r}_2. \tag{2.30}$$

$T_s[\rho]$ is noninteracting kinetic energy. Its detail is explained elsewhere [7]. The first theorem considers the two similar systems acted by difference external potentials, $v(\mathbf{r})$ and $v'(\mathbf{r})$. Each system has its Hamiltonian, H, H', eigenenergy, E, E', and eigenstate, Ψ, Ψ', which has the same density, $\rho(\mathbf{r})$ both (only $v(\mathbf{r}) - v'(\mathbf{r}) \neq$ const). We can write the equations

$$E < \langle\Psi'|H|\Psi'\rangle = \langle\Psi'|H' + V_{ext} - V'_{ext}|\Psi'\rangle, \tag{2.31}$$

$$E < E' + \int (v - v')\rho(\mathbf{r})d\mathbf{r}, \tag{2.32}$$

and vice versa,

$$E' < E + \int (v' - v)\rho(\mathbf{r})d\mathbf{r}. \tag{2.33}$$

From Eq 2.32 and Eq 2.33, they give

$$E + E' < E + E', \tag{2.34}$$

so two systems with difference external potentials will be conflicted to have the same density. It is proved that the density is unique to a given external potential. This theorem makes us confidence that the density will be solved is the ground state density, $\rho(\mathbf{r}_0)$, of the regarded systems. The second theorem is that the $\rho_0(\mathbf{r})$ will give the ground state energy, E_0, which is the lowest one. If there is the density, $\tilde{\rho}(\mathbf{r})$, which is not the ground state density, it will give energy higher than the ground state energy,

$$E_0 = E[\rho_0(\mathbf{r})] \leq E[\tilde{\rho}(\mathbf{r})]. \tag{2.35}$$

2.3.3 Kohn-Sham method

The Hartree-Fock wave function gives only the exchange term thus, the energy does not contain by the correlation energy. The density matrices come to play the central role of this problem,

$$\rho_N(\mathbf{r}'_1\mathbf{r}'_2\cdots\mathbf{r}'_N,\mathbf{r}_1\mathbf{r}_2\cdots\mathbf{r}_N)=\Psi_N(\mathbf{r}'_1\mathbf{r}'_2\cdots\mathbf{r}'_N)\Psi^*_N(\mathbf{r}_1\mathbf{r}_2\cdots\mathbf{r}_N). \tag{2.36}$$

The Eq 2.36 involves with many variables that difficult to solve, so it should be reduced into one particle problem as,

$$\rho_1(\mathbf{r}'_1,\mathbf{r}_1)=N\int\cdots\int\rho_N(\mathbf{r}'_1\mathbf{r}_2\cdots\mathbf{r}_N,\mathbf{r}_1\mathbf{r}_2\cdots\mathbf{r}_N)d\mathbf{r}_2\cdots d\mathbf{r}_N. \tag{2.37}$$

For the Coulomb potential, there are two electrons interacting, so it needs the reduced density matrices for two particles problem,

$$\rho_2(\mathbf{r}'_1\mathbf{r}'_2,\mathbf{r}_1\mathbf{r}_2)=\frac{N(N-1)}{2}\int\cdots\int\rho_N(\mathbf{r}'_1\mathbf{r}'_2\mathbf{r}_3\cdots\mathbf{r}_N,\mathbf{r}_1\mathbf{r}_2\mathbf{r}_3\cdots\mathbf{r}_N)d\mathbf{r}_3\cdots d\mathbf{r}_N. \tag{2.38}$$

The Hamiltonian in the form of the density functional can be written as Eq 2.37. The Coulomb potential will be less complicated when the density matrices is reduced to one particle density matrices,

$$J[\rho]=\frac{1}{2}\int\frac{1}{r_{12}}\rho(\mathbf{r}_1)\rho(\mathbf{r}_2)d\mathbf{r}_1d\mathbf{r}_2. \tag{2.39}$$

Eq 2.39 is the Hartree potential that contains only the classical part of Coulomb potential. Therefore, the reduce density matrices for two particles can be written as,

$$\rho_2(\mathbf{r}'_1\mathbf{r}'_2,\mathbf{r}_1\mathbf{r}_2)=\frac{1}{2}[\rho(\mathbf{r}_1)\rho(\mathbf{r}_2)+\rho(\mathbf{r}_1)\rho_{xc}(\mathbf{r}_1,\mathbf{r}_2)], \tag{2.40}$$

which is separated into two parts, classical part and quantum part. The ρ_{xc} is the exchange-correlation hole which gives the exchange-correlation energy,

$$E_{xc}[\rho]=\frac{1}{2}\iint\frac{1}{r_{12}}\rho(\mathbf{r}_1)\rho_{xc}(\mathbf{r}_1,\mathbf{r}_2)d\mathbf{r}_1d\mathbf{r}_2. \tag{2.41}$$

The energy functional in Eq 2.27 becomes

$$E[\rho]=T_s[\rho]+J[\rho]+E_{xc}[\rho]+V_{ext}[\rho]. \tag{2.42}$$

According to Hohenberg-Kohn second theorem we need the variational method to find the extremum path

$$\frac{\delta E[\rho]}{\delta\rho(\mathbf{r})}=0, \tag{2.43}$$

then

$$\int\delta\rho(\mathbf{r})\Big\{-\frac{1}{2}\nabla^2+v_{eff}(\mathbf{r})\Big\}d\mathbf{r}=0, \tag{2.44}$$

when

$$v_{eff}(\mathbf{r}) = \int \frac{\rho(\mathbf{r}')}{|\mathbf{r}-\mathbf{r}'|} d\mathbf{r}' + v(\mathbf{r}) + \frac{\delta E_{xc}[\rho]}{\delta \rho(\mathbf{r})}. \tag{2.45}$$

The $v_{eff}(\mathbf{r})$ is the effective potential that the noninteracting electron are moving in. Therefore, the $\rho(\mathbf{r})$ is satisfied the Eq 2.43, Eq 2.44 and Eq 2.45 can be solved by one-particle Schrödinger equation (in atomic unit)

$$\Big\{ -\frac{1}{2}\nabla^2 + v_{eff}(\mathbf{r}) \Big\} \psi_i^{KS}(\mathbf{r}) = \varepsilon_i \psi_i^{KS}(\mathbf{r}), \tag{2.46}$$

when

$$\rho(\mathbf{r}) = \sum_{i=1}^{N} |\psi_i^{KS}(\mathbf{r})|^2. \tag{2.47}$$

The ψ_i^{KS} is the Kohn-Sham orbital. The $\rho(\mathbf{r})$ can be solved self-consistently by the Eq 2.45, Eq 2.46 and Eq 2.47 which is known as the Kohn-Sham method [8].

2.4 Techniques of Calculation on DFT

Even the DFT was approximated for easy solving the solution of the one-particle Schrödinger equation, however, the electron wave function is opened to be any completeness basis sets and an exact form of the exchange-correlation energy is still a missing puzzle. There are many solutions for these problems but they are differed by the speed of calculation, the accuracy and the precision. In CASTEP code used in this thesis, we used the plane wave (PW) basis set with pseudopotential method. The exchange-correlation energy used both the local density approximation (LDA) and the generalized gradient approximation (GGA) in our calculation.

2.4.1 Plane Wave basis set

The atoms in solid state arrange orderly and has periodicity. If we consider the noninteracting electron, it is acted by only the background potential from the nucleus which is formed the crystal. The potential has to follow the Bloch's theorem

$$U(\mathbf{r}) = U(\mathbf{r}+\mathbf{T}), \tag{2.48}$$

where $\mathbf{T}$ is a translation vector that the electrons are acted, by the potential, the same for the initial and final positions. The $U(\mathbf{r})$ satisfies the periodicity in solid by this condition. The electron wave function follows the Bloch's theorem is

$$\Psi(\mathbf{r}+\mathbf{R}) = e^{i\mathbf{k}\cdot\mathbf{R}}\Psi(\mathbf{r}). \tag{2.49}$$

The electrn wave functions can be written in the Fouriers form which satisfy the Bloch's theorem as

$$\Psi(\mathbf{r}) = \frac{1}{\Omega}\sum_{m}\Psi(\mathbf{k}+\mathbf{G}_m)e^{i(\mathbf{k}+\mathbf{G}_m)\cdot\mathbf{r})} \tag{2.50}$$

where Ω is the volume of the solid and $\mathbf{G}$ is the reciprocal lattice vector.

2.4.2 Pseudopotential method

The calculation of all electron (AE) wave function in solid gives the best accuracy but is very cumbersome. However, the AE wave function can be separated into two parts, the core and valence wave function as suggested by Herring [9], Phillips and Kleinman [10]. The valence wave function in core region divided by core radius (r_c) oscillates that make the laborious calculation. In contrast to the valence wave function which is smooth part that does the chemical bond and distributes at the Fermi surface. It is easier to avoid calculating the core region and perform accurate calculation in smooth part by using a pseudo wave function

$$|\psi_{ps}\rangle = |\psi\rangle - \sum_{c}|\psi_c\rangle\langle\psi_c|\psi_{ps}\rangle, \tag{2.51}$$

where ψ_c is the wave function in core region, so the summation is summed over the core states and ψ is the AE wave function. The Schrödingers equation that satisfies the pseudo wave function is

$$H|\psi\rangle = E|\psi\rangle, \tag{2.52}$$

$$H(|\psi_{ps}\rangle + \sum_{c}|\psi_c\rangle\langle\psi_c|\psi_{ps}\rangle) = E(|\psi_{ps}\rangle + \sum_{c}|\psi_c\rangle\langle\psi_c|\psi_{ps}\rangle), \tag{2.53}$$

$$H|\psi_{ps}\rangle + \sum_{c}(E_c - E)|\psi_c\rangle\langle\psi_c|\psi_{ps}\rangle = E|\psi_{ps}\rangle, \tag{2.54}$$

where $H = -\frac{1}{2}\nabla^2 + V(\mathbf{r})$ and E_c is the eigenenergy of the core state, so that

$$(-\frac{1}{2}\nabla^2 + U_{ps})|\psi_{ps}\rangle = E|\psi_{ps}\rangle, \tag{2.55}$$

where $U_{ps} = V(\mathbf{r}) + \sum(E_c - E)|\psi_c\rangle\langle\psi_c|$ is the pseudopotential. Eq 2.55 advantages that E can be calculated by using the pseudo wave function and pseudopotential instead of the AE wave function. Fig 2.5 shows that the real wave function is cut the oscillating part inside the r_c and replaced with the smooth part of the pseudo wave function.

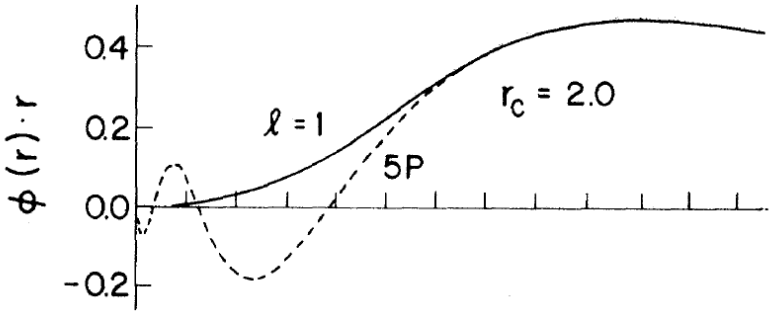

Figure 2.5: The comparison between the AE wave function (dash line) and the pseudo wave function (solid line) of molybdenum. [11]

There are the conditions that make an accurate pseudo wave function. Hamann, Schlüter and Chiang proposed the conditions (known as norm-conserving pseudopotential) [11] that the pseudo wave function has to follow the properties:

1. The eigenvalues of the real and pseudo systems, E and E', respectively, are equivalent

$$E = E'. \tag{2.56}$$

2. The wave functions outside the core region of the real and pseudo systems are equivalent

$$\psi(\mathbf{r}) = \psi_{ps}(\mathbf{r}) \text{ for } r \geq r_c. \tag{2.57}$$

3. The integrals from 0 to R, when $R > r_c$, of the real and pseudo charge densities are equivalent (norm-conserving)

$$\langle\psi|\psi\rangle_R = \langle\psi_{ps}|\psi_{ps}\rangle_R. \tag{2.58}$$

4. The first energy derivatives of the logarithmic derivatives of the real and pseudo wave function are equivalent for $r > r_c$.

The norm-conserving pseudopotentials conditions are too restricted and are inappropriate for some systems. Vanderbilt showed that removing the norm-conserving constraint can reduce the numbers of plane waves in our calculation and also increase the speed of calculation [12]. It is so-called ultrasoft pseudopotential.

2.4.3 Exchange-correlation energy

The Eq 2.41 is left with complicated that there is no exact form. There are many approximations for this term. Two acceptable approximations that have the high

accuracy for calculation the physical property (i.e. lattice parameters, phonon) and are most popular are the LDA and the GGA. They are difference in physics idea. The LDA bases on the homogenous electron gas

$$E_{xc}[\rho] = \int \rho(\mathbf{r})\epsilon_{xc}(\rho)d\mathbf{r}, \tag{2.59}$$

where $\epsilon_{xc}(\rho)$ is the exchange-correlation energy density. In CASTEP code, it is modeled by Ceperley and Alder [13] and is parameterized by Perdew and Zunger [14] which the details are shown in Appendix C. But the electrons are not really uniform, so the inhomogenous electron gas is regarded. The GGA takes the gradient term of the density matrices into account

$$E_{xc}[\rho] = \int \rho(\mathbf{r})\epsilon_{xc}(\rho, \nabla\rho)d\mathbf{r}. \tag{2.60}$$

This work used the Perdew, Burke and Ernzerhof [15] model which its detail is shown in Appendix C.

Chapter III

METHOD

We used CASTEP (CAmbridge Serial Total Energy Package) code [16] which is hosted by Materials Studio (MS) program to calculate the energy and the properties of scandium trihydride. CASTEP is based on DFT and uses the plane-wave basis set and pseudopotential method. There are many advantages to predict the properties of materials or even molecules, such as, the lattice parameters, bulk modulus, phonons, density of states, band structure, charge densities, atomic populations, and optical properties etc. In this chapter, we will describe the detail of building the structure i.e. hcp phase, fcc phase, and intermediate phase. The BFGS (Broyden-Fletcher-Goldfarb-Shanno) scheme and the on the fly pseudopotential are chosen in calculation. The parameters energy cutoff and **k**-point meshes are also chosen for the convergence of the energy.

3.1 The hcp and fcc phases

From Chapter I, there were experiments which identified the hcp phase of the ScH_3. The metal planes are formed as the pattern ABABAB and it is the hcp phase which was showed clearly by XRD and neutron experiments. The neutron experiment showed the structure of ScH_3 by assuming the $P6_3/mmc$ symmetry structure to the neutron diffraction pattern. The atomic positions are shown in Table 1.1. The scandium atom is at $2c$ site which stays at $(\frac{1}{3}, \frac{2}{3}, \frac{1}{4})$ position. The hydrogen atoms are more complicated. The H_t atom is displaced from the ideal T site to the $4f$ site which stays at $(\frac{1}{3}, \frac{2}{3}, -0.088)$ position. The H_m atom is displaced from the metal plane to the $4e$ site which stays at $(0, 0, 0.210)$ position. We note that there is only one H_m atom in the unit cell but by filling atom at $4e$ site gives two H_m atoms. Therefore, it should be only half of the H_m which can be filled in this site, or to be exact has 0.48 occupancy. The experimentalists suggested that the H_m atoms distribute randomly around their sites, however, the random

distribution uses enormous resources in calculations. We assume that they are stationary at their position as shown in Fig 3.1a.

This structure has the $P3m1$ symmetry but is not the lowest energy structure. From the geometry optimization, the H_m atoms can move to the metal planes and lower the energy by 0.01 eV. The symmetry is then changed to $P6_3/mmc$. Nevertheless, we choose to strict to the experimental structure, so the H_m atomic positions are fixed while the structure is being optimized. The fcc structure is very simple and it is the $Fm\bar{3}m$ symmetry structure. The scandium atom is placed at $4a$ site which locates at (0,0,0) position. There are two hydrogen atoms placed at T sites which are the $8c$ sites and at $(\frac{1}{2}, \frac{1}{2}, \frac{1}{2})$ position and at O sites which is the $4b$ site and at $(\frac{1}{4}, \frac{1}{4}, \frac{1}{4})$ position. The structure of fcc is shown in Fig 3.1b.

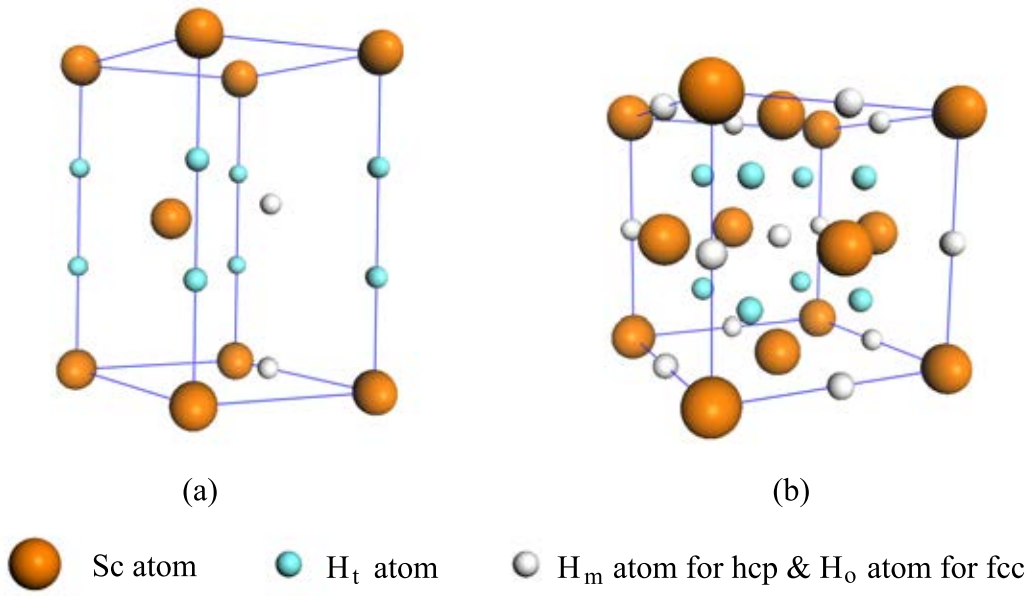

Figure 3.1: The structure model of ScH_3 (a) hcp phase and (b) fcc phase.

3.2 Convergence test

The crystal is periodic, so we can consider only one unit cell instead of the whole bulk. The boundary of the reciprocal primitive unit cell is at the Brillouin zone boundary. The smallest regarded system can reduce the cost of calculation. The Brillouin zone is build in the same way as the Wigner-Seitz cell. The walls of the zone are perpendicular to the reciprocal space vector, **G**, and cross at the

half which constitute the first Brillouin zone. However, the first Brillouin zone is not enough for consideration because the second and others Brillouin zones have higher energy. On the other hand, the Fourier form of the wave function in Eq 2.50 is summed cumulatively due to the high order of the Brillouin zone that leads to longer computational time. We can find the appropriate value of **G** that makes the converged solution when the **G** related to the energy by

$$E_c = \frac{\hbar^2}{2m} G_{max}^2, \tag{3.1}$$

where E_c is the cutoff energy and G_{max} which is the maximum reciprocal space that the plane wave is summed over. Fig 3.2 shows that the reciprocal space can be divided into k-point mesh which is proposed by Monkhorst and Pack [17, 18]

$$k_i = \frac{2q_i - p_i - 1}{2p_i} \;\; ; \;\; q_i = 1, 2, \ldots, p_i \;\; , \tag{3.2}$$

where p_i is the amount of k-point in i direction and k_i is the distance to the q^{th} position in reciprocal space. The finer k-point mesh affects the convergence of the energy.

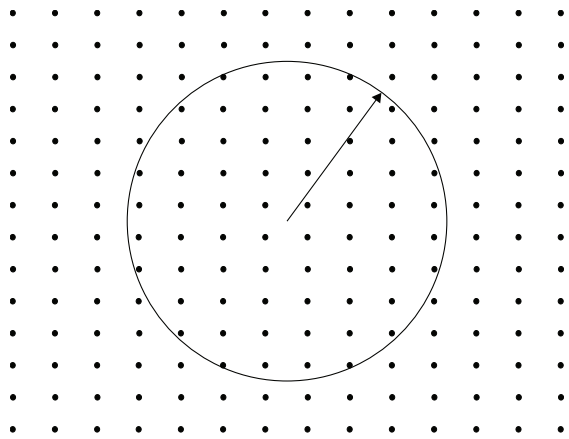

Figure 3.2: The k-point mesh expand all reciprocal space where the circle is the cutoff of the calculation.

The convergence tests of E_c and k-point separation k_s are shown in Fig 3.3. We tested the parameters for the hcp and fcc phases that yield the same results. The energy cutoff of 650 and 700 eV yield slightly better convergent energy than of 600 eV, but they are rather time consuming, so the appropriate E_c for both phases is 600 eV (see Fig 3.3a,c). We chose the $k_s = 0.02$ Å for both phases which is give the good convergent energy. Noting that for the intermediate phase the calculation used $k_s = 0.04$ Å because system size is rather big results in taking more computation time.

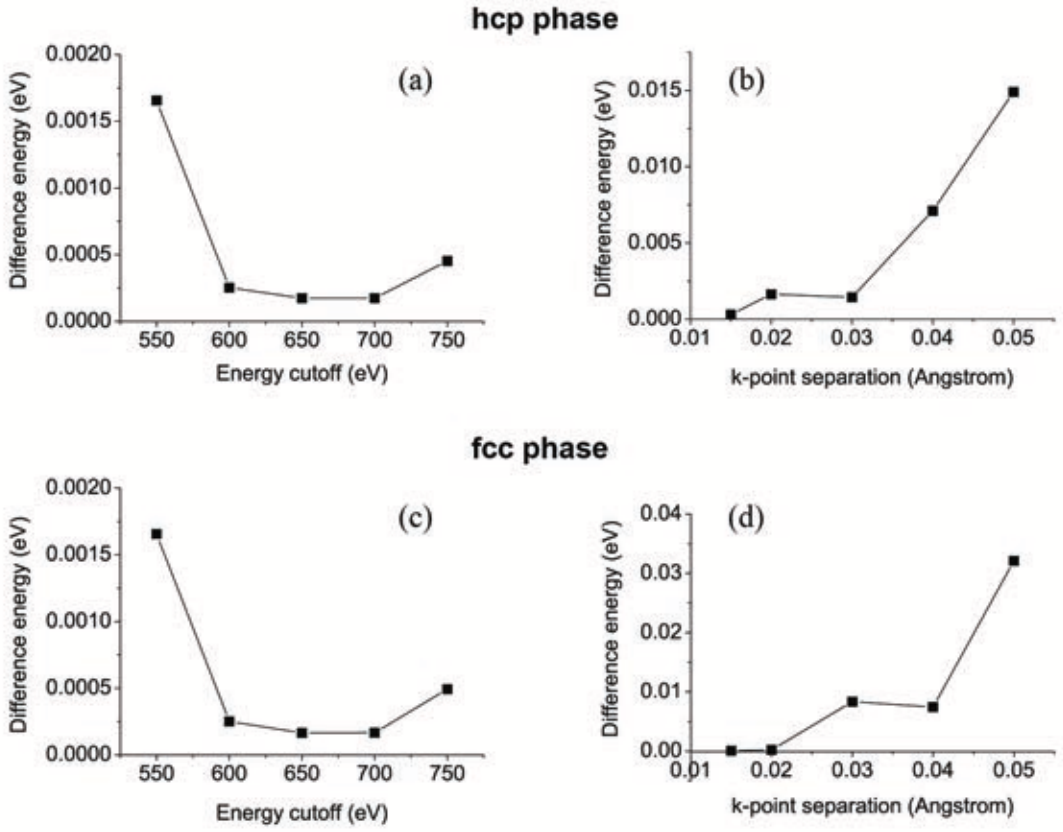

Figure 3.3: (a)&(b) are the convergence test of hcp phase for energy cutoff and k-point separation, respectively. (c)&(d) are the convergence test of fcc phase for energy cutoff and k-point separation, respectively. The y-axis is the difference energy that differs averagely from finer and coarser x-axis values.

3.3 Geometry Optimization

The geometry optimization is the method that searches for the ground state crystal structure [19]. The unrelaxed crystal structure can be relaxed, by this method, to satisfy the applied external potential. We know, from Chapter II, that the system which is in contact with pressure and 0 K reservoirs prefers the minimum enthalpy

$$\mathcal{H} = E + P\Omega. \tag{3.3}$$

The enthalpy is the functional of $(9 + 3N)$-dimensional space where 9 are of the strain components and $3N$ are of the coordinates of atoms

$$\mathcal{H} = \mathcal{H}(\epsilon, \mathbf{r}_1, \mathbf{r}_2, \ldots, \mathbf{r}_N). \tag{3.4}$$

The force vector can be calculated by the first derivative of the enthalpy respect to X

$$F = -\frac{\partial \mathcal{H}}{\partial X}\bigg|_P, \tag{3.5}$$

where

$$X_{3(i-1)+j} = \epsilon_{ij} \ \ ; \ \ i,j = 1,2,3 \ \ , \tag{3.6}$$

and the followers are the coordinate of the atoms

$$X_i = \mathbf{r}_i \ \ ; \ \ i = 1,2,\ldots,N \ \ . \tag{3.7}$$

The variation of enthalpy around the minimum X_{min} is

$$\delta\mathcal{H} = \frac{1}{2}(X - X_{min}) \cdot B(X - X_{min}), \tag{3.8}$$

where B is the Hessian matrix. The quasi-Newton method* which is a root finding algorithm help us to search for the X_{min} from the F in one relaxation step. The X_k will be improved to the X_{min} by the equation

$$\Delta X_k = H_k F_k, \tag{3.9}$$

where $H = B^{-1}$. H_0 is unknown but it can be guessed and updated by the BFGS method. When the X reaches its minimum, the crystal structure satisfies the external pressure and it also has the minimum enthalpy which is calculated from the above algorithm. In this work, we calculated the enthalpy of the hcp and fcc phases every 5 GPa from 0 to 60 GPa. The result will be discussed in Chapter IV.

3.4 On the fly pseudopotential

The on the fly pseudopotential was used. It is based on either the norm-conserving pseudopotential or the ultrasoft pseudopotential. In CASTEP code, the developers improve the pseudopotentials that can be the softer or harder potentials by changing the core radius. In this work, we used 11 valence electrons for scandium atom and choose the on the fly bases on the ultrasoft pseudopotential. The electron configuration is $3d^1 \ \ 4s^2 \ \ 3p^6 \ \ 3s^2$.

3.5 The model of the intermediate phase

The intermediate phase discussed in Chapter IV is the stacking sequence of the layers that could be changed from ABABAB to ABCABC by sliding the $(001)_h$ planes in $[110]_h$ and $[1\bar{1}0]_h$ directions. Because the crystal is periodic, so the

*see Appendix D

completed transformation needs at least three unit cells in the c-axis as shown in Fig 3.4. The displacement of the sliding layers from one void to another void is proved in Eq 2.4. The layers of the intermediate phase are stacked among AB to CA and AB to BC, so the displacement of each step of the sliding layers can be calculated by dividing the Eq 2.4 by the number of step, n

$$d = \frac{\sqrt{3}}{3}\frac{a}{n}. \tag{3.10}$$

There are only metal planes that are slid and left the hydrogen atoms at their initial positions for every steps (see Fig 3.4). The metal planes are fixed after they were slid. The hydrogen atoms are relaxed while the structure is being optimized. The results will be shown in Chapter IV.

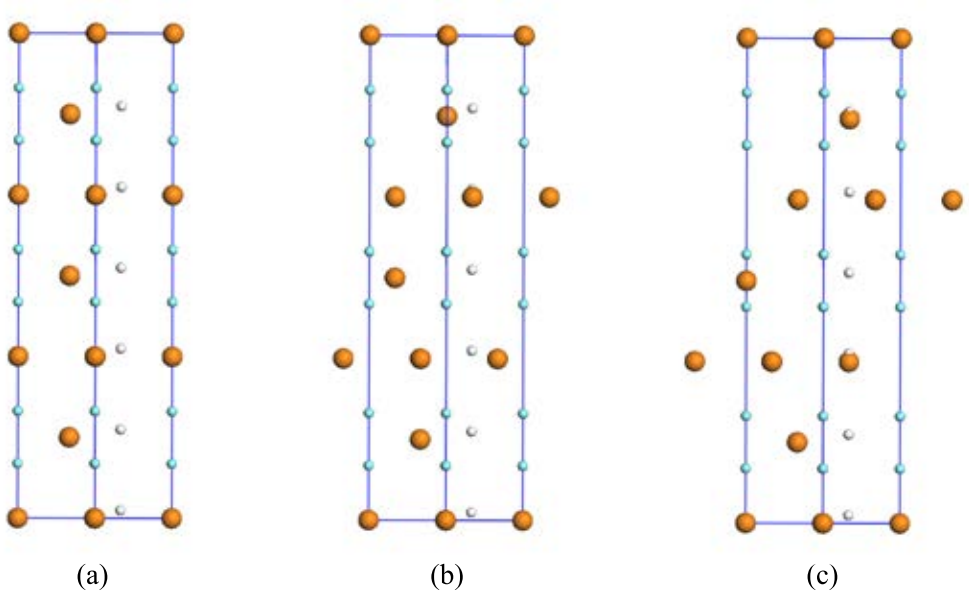

Figure 3.4: The models are shown the side that parallels to the $(110)_h$ plane. (a) The $3 \times 1 \times 1$ supercell of hcp phase. (b) The intermediate step of sliding layers. (c) The last step of sliding layers.

Chapter IV

RESULTS AND DISCUSSIONS

In experiment, scandium trihydride which formed only under pressure has the hcp phase. Its structure is changed to the intermediate phase when the pressure reaches 25 GPa subsequently it transforms to the fcc phase around 46 GPa. The intermediate phase dominates in a range of 25 GPa $\rightarrow$ 46 GPa. It is the phase between hcp and fcc phases and has been unidentified for the exact structure. The main point of this work is to identify the structure of this intermediate phase in order to fulfill the phase diagram. To understand the intermediate phase, we need to know the structure of the hcp and the fcc phases. From Chapter 1, the structure of the hcp phase is reported in the experiment to be in the space groups $P6_3/mmc$. The scandium atoms are placed at the hcp positions. The hydrogen atoms are placed near the T sites and the M sites. The structure of the fcc phase is in the space groups $Fm\bar{3}m$. The scandium atoms are placed at the fcc positions. The hydrogen atoms are placed on the T sites and the O sites. The information that helps us to identify the intermediate phase is the d-spacing. From the d-spacing, we believe that the structure transforms continuously from the hcp phase to the fcc phase. Therefore the hcp and the fcc phases are the initial and the final structures of the intermediate phase, respectively. The main aim of this thesis is to propose the atomic structure of the intermediate phase, then some physical quantities such as d-spacing and molar volume will be compared with available experimental results.

4.1 The intermediate phase

The experiment showed the continuity and splitting of the d-spacing of the hcp phase to intermediate phase to the fcc phase. The $(101)_h$ plane splits into two planes at the intermediate phase which are the d5 and the d6 plane in Fig 1.1(a). The d5 plane transforms to the $(111)_f$ plane and the d6 plane transforms to the $(200)_f$ plane. The $(110)_h$ decreases continuously to be the d7 plane in Fig 1.1(a) of

the intermediate phase and the $(220)_f$ plane of fcc phase, respectively. These are the main key suggest what is the intermediate phase look like. There are two kinds of the structure that could be the intermediate phase. The first is the distinguishable symmetry structure that is static while the pressure increases such as bcc, sc, etc. The second is the structure stuck during the transformation from the hcp phase to the fcc phase and is variable basis while the pressure increases. However, the d-spacing at d5 plane increases at the beginning but it decreases at the later transformation. It is very special that there is both increasing and decreasing of the d-spacing for any plane of any structure under pressure. On the one hand, two statical structure can explain the behavior of the d5 plane but they cannot explain the behavior d6 and d7 plane that their d-spacings decrease continuously. Therefore, the intermediate phase is possibly a variable basis structure.

The hydrogen atoms are not detected by XRD, so the d-spacing are of the scandium atoms only. The scandium atoms in the hcp phase form the close packing structure in the pattern ABABAB. It has many ways to transform to the fcc phase i.e. the pattern ABCABC, but the transformation is constrained by the d-spacing. The $(110)_h$ plane must be conserved because the d-spacing decreases continuously even at the phase changes. In another word, the $(110)_h$ plane is conserved when the structure transforms to the fcc phase and becomes the $(220)_f$ plane. If the atoms move on the $(110)_h$ plane while the structure is transforming, this plane will be conserved (see Fig 4.1a). From Chapter 2, the easiest way to transform from the hcp phase to the fcc phase is to rearrange the 6 layers of the close packing ABABAB layers. The 3^{rd} and 4^{th} layers slide from AB to CA in the $[1\bar{1}0]_h$ direction and the 5^{th} and 6^{th} layers slide from AB to BC in the $[\bar{1}10]_h$ direction. Therefore, we have fcc pattern ABCABC of which the $(110)_h$ plane is conserved. Moreover, the $(110)_h$ plane becomes the $(220)_f$ plane (see Fig 4.1b,c). The scandium atoms placed between the $(110)_h$ planes are compressed by pressure and the d-spacing value decreases without destroying the planes that corresponding to the experimental findings. Now, we know that this is the transformation mechanism. The question is what are the d5, d6 and d7 planes. To see these planes clearly, we have to examine the transformation mechanism in more detail. The atomic distance that slide to change the stacking position is one-third of longer diagonal of rhombus or can be calculated by Eq 2.4. When the structure distorts, it loses the $P3m1$ symmetry. The hcp pattern is periodic every 3 layers of scandium atoms, but after the distortion the new structure is periodic every 7 layers of scandium atoms and has the space group Cm (see Fig 4.2). The $(110)_h$ plane in the hcp phase is equivalent to the $(020)_{Cm}$ plane in Cm phase.

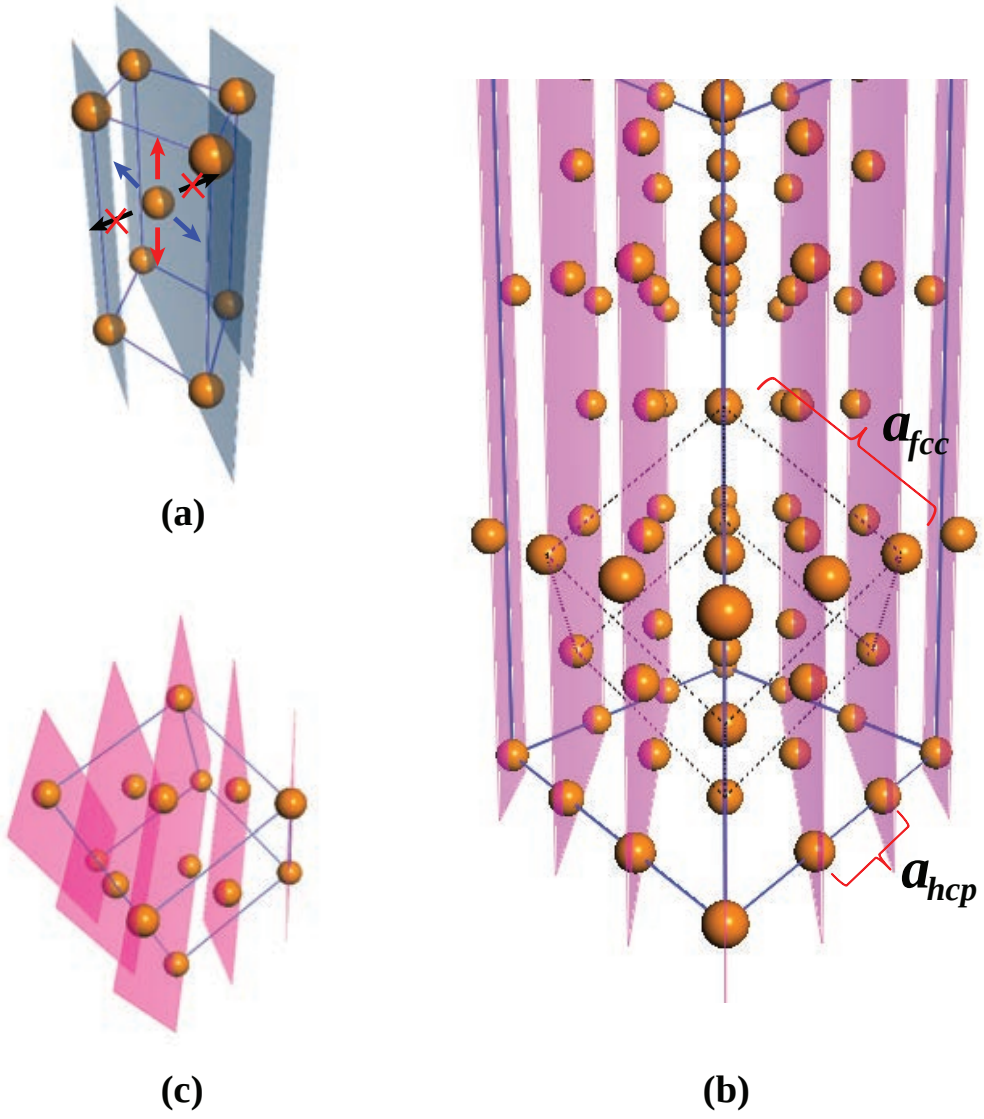

Figure 4.1: (a) The figure shows the hcp unit cell along with the $(110)_h$ planes. The atom can move on the $(110)_h$ plane only which is the direction of the red and blue arrows. The atom cannot move in the black arrow direction because the $(110)_h$ will be demolished. (b) A fcc unit cell (black dash cubic) is embedded in the hexagonal system enclosed in the blue line. The $(110)_h$ planes in hexagonal system (pink planes) cut through the atoms on the fcc system that is equivalence to the $(220)_f$ planes. (c) The $(220)_f$ planes cut through the atoms on cubic system.

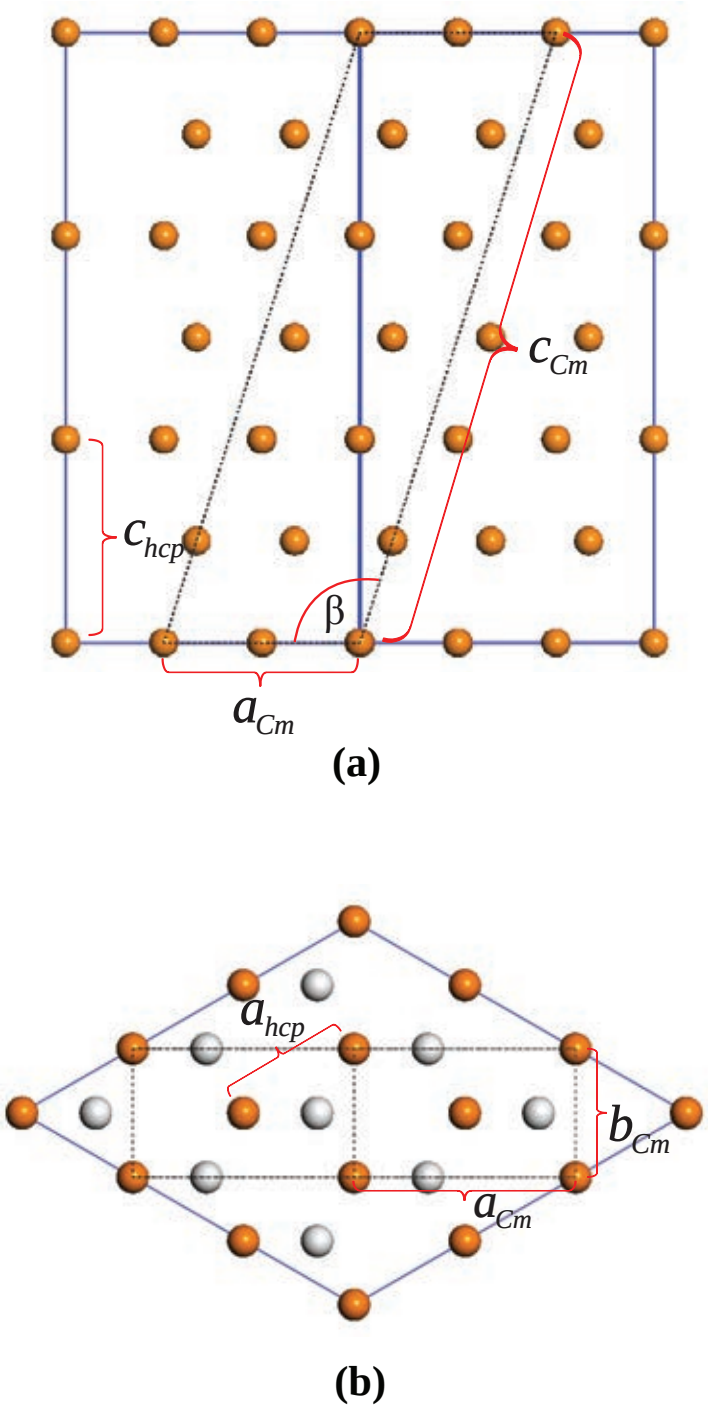

Figure 4.2: The Cm unit cell contains a $3 \times 3 \times 3$ hexagonal supercell. the projection on the $(110)_h$ plane is represented by black dash lines. The atoms are arranged as the hcp pattern. (a) The Cm unit cell is projected on the $(110)_h$ plane. (b) The top view of the Cm unit cell.

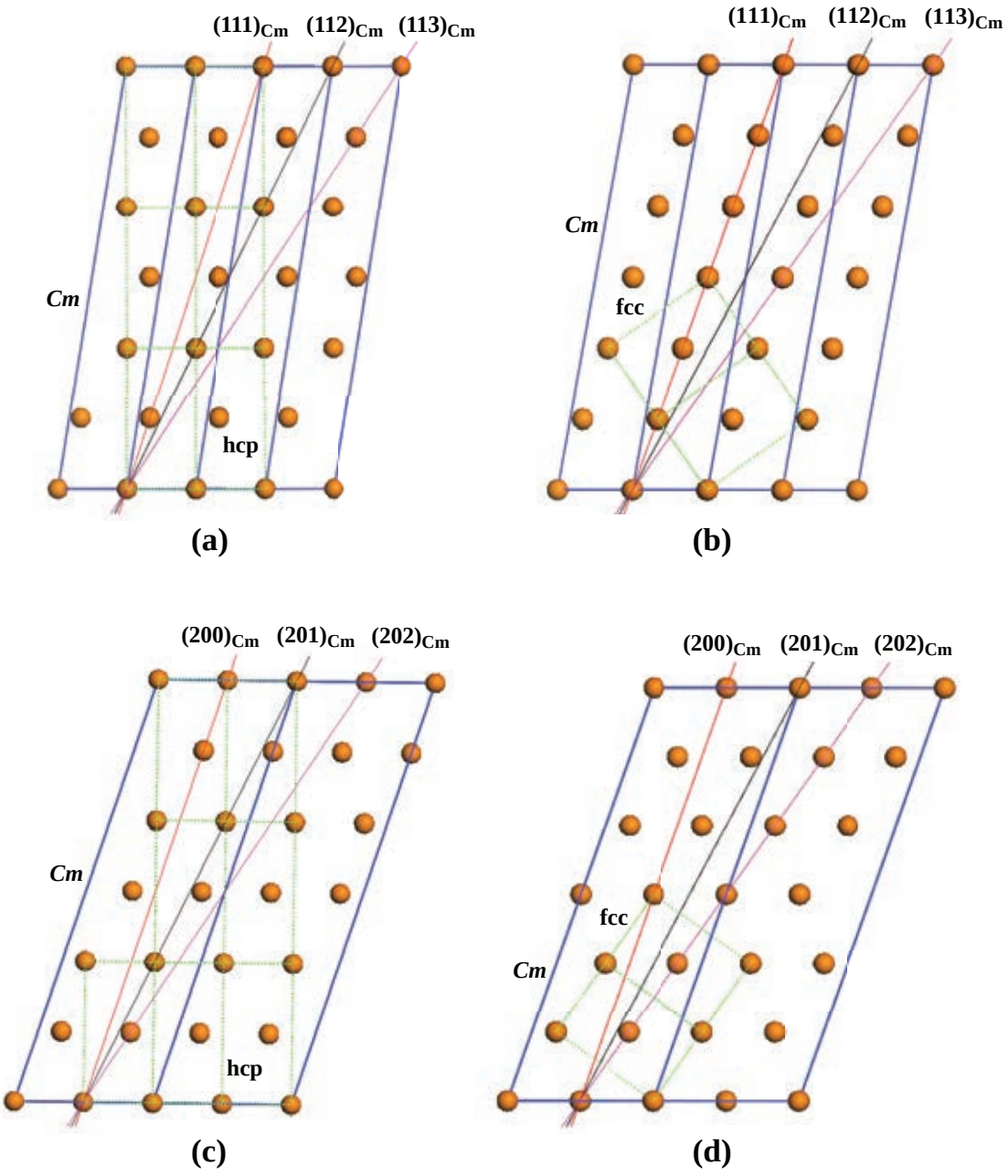

Figure 4.3: The figures show the Cm structure. For simplicity, only the scandium atoms are shown. (a) the projection of the hcp phase onto the $(010)_{Cm}$ plane. The $(201)_{Cm}$ is equivalent to the $(1\bar{1}1)_h$ plane. (b) the projection of the fcc phase onto the $(010)_{Cm}$ plane. The $(202)_{Cm}$ is equivalent to the $(200)_f$ plane. (c) the projection of the hcp phase onto the $(\bar{3}10)_{Cm}$ plane. The $(112)_{Cm}$ plane is equivalent to the $(101)_h$ plane. (d) the projection of the fcc phase onto the $(\bar{3}10)_{Cm}$ plane. The $(111)_{Cm}$ plane is equivalent to the $(111)_f$ plane. The hcp unit cells are indicated by green boxes in (a) and (c). The fcc unit cells are indicated by green boxes in (b) and (d). Other essential planes are guided by colored lines.

The structure transforms pass through the Cm phase with conserving the $(020)_{Cm}$ plane and then it ends up at the fcc phase. The $(020)_{Cm}$ plane transforms to the $(220)_f$ plane at last. Therefore, the d7 plane is the $(020)_{Cm}$ plane. The Cm phase can be used to identify the d5 and d6 plane, also. Fig 4.3 shows the $(101)_h$ and $(111)_f$ planes can be mapped on the plane of the Cm phase to be the $(112)_{Cm}$ and $(111)_{Cm}$ planes, respectively.

The Cm can be used to show the linkage between the fcc and the hcp phases and the $(101)_h$ plane becomes the $(111)_f$ plane by the dispersion of $(112)_{Cm}$ to $(111)_{Cm}$ planes. Therefore, the d5 plane is the plane between $(112)_{Cm}$ and $(111)_{Cm}$ planes. For the d6 plane, The d-spacing between the $(1\bar{1}1)_h$ and $(101)_h$ planes are proved by the equation of hexagonal system in Table 2.1 that they are equivalence, so the $(1\bar{1}1)_h$ plane has been hidden in the d-spacing information. This plane will become the d6 plane. From Fig 4.3, It shows that the $(1\bar{1}1)_h$ and $(200)_f$ planes are mapped on the plane of the Cm phase which are the $(201)_{Cm}$ and $(202)_{Cm}$ planes, respectively. It is the same as in the d5 plane. The d6 planes is the dispersion of the $(201)_{Cm}$ to $(202)_{Cm}$ planes. The mechanism of transformation of scandium atoms from the hcp phase to the fcc phase can be well described by the dispersion of the Cm planes. However, the hydrogen atoms have more complicated transformation and cannot be described by the analysis from the d-spacing information. It will be discussed in next section.

4.2 fcc form on hexagonal system

The close packing layers are perpendicular to the $[001]_h$ direction. Different stacking sequences cause the hcp phase and the fcc phase. The c axis of the hcp phase is parallel to the $[001]_h$, so it aligns normally on the hexagonal system. The fcc phase can be viewed as "a cubic stands on its corner" on the hexagonal system. Three corner atoms which are on the $(111)_f$ plane stay at the same height of the hexagonal system (see Fig 4.4). This relation can be written in the equation as,

$$z_{hcp} = z_{hcp}(x_{fcc}, y_{fcc}, z_{fcc}), \tag{4.1}$$

$$z_{hcp}(a_{fcc}, 0, 0) = z_{hcp}(0, a_{fcc}, 0) = z_{hcp}(0, 0, a_{fcc}), \tag{4.2}$$

where the a_{fcc} is the lattice parameters of the fcc phase. The subscript "hcp" refers to the coordinate of hcp phase and the subscript "fcc" refers to the coordinate of the fcc phase. The coordinates in fcc phase can be transformed to coordinates in the hexagonal system by rotating the z_{fcc} axis as an angle 45°, and then the x'_{fcc}

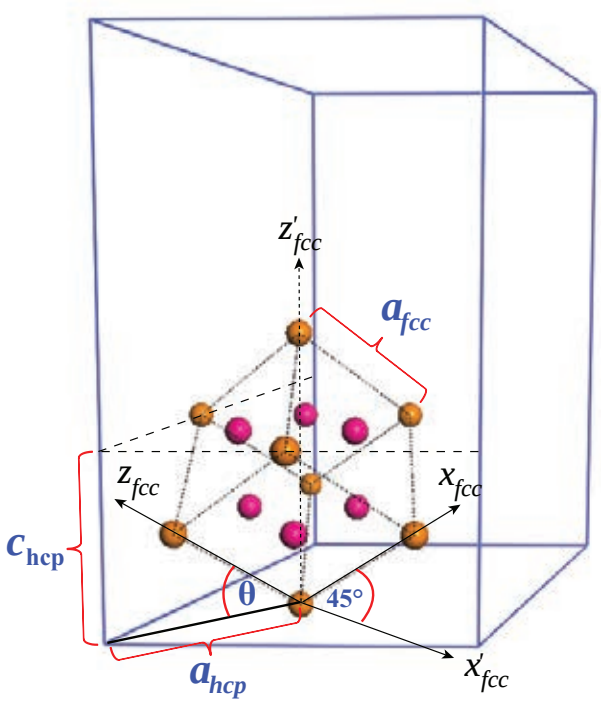

Figure 4.4: The figure shows that how the fcc phase relies on hexagonal system with the rotation axis.

axis is rotated by the angle $90° - \theta$ (see Fig 4.4). Therefore, the coordinate of the fcc phase can be transformed into the coordinate in the hexagonal system by using Euler angles,

$$\mathbf{x}_{hcp} = R_{x'_{fcc}}(90° - \theta) R_{z_{fcc}}(45°) \mathbf{x}_{fcc}, \tag{4.3}$$

$$\begin{pmatrix} x_{hcp} \\ y_{hcp} \\ z_{hcp} \end{pmatrix} = \frac{1}{\sqrt{2}} \begin{pmatrix} 1 & -1 & 0 \\ \sin\theta & \sin\theta & -\sqrt{2}\cos\theta \\ \cos\theta & \cos\theta & \sqrt{2}\sin\theta \end{pmatrix} \begin{pmatrix} x_{fcc} \\ y_{fcc} \\ z_{fcc} \end{pmatrix}. \tag{4.4}$$

Fig 4.4 shows that the atom at $(0, 0, 1)_{fcc}$ tilts down by an angle θ with the ground, and then it locates at $(\frac{1}{3}, \frac{1}{6}, \frac{1}{2})_{hcp}$. Accordingly, the angle θ can be written as

$$\theta = \arctan\left(\frac{\sqrt{3}c_{hcp}}{4a_{hcp}}\right). \tag{4.5}$$

The relation between lattice parameters of the hcp and the fcc phases is

$$a_{fcc} = \sqrt{\frac{4a_{hcp}^2}{3} + \frac{c_{hcp}^2}{4}}. \tag{4.6}$$

By including Eq 4.4, Eq 4.5 and Eq 4.6, the coordinate of the hcp phase can be

Table 4.1: The height of the hydrogen atoms of the fcc form placed in the hexagonal system.

hydrogen atoms	x_{fcc}	y_{fcc}	z_{fcc}	$z_{hcp} \times \frac{a_{fcc}}{c_{hcp}}$
H_t atoms	1/2	0	0	2/8
	1/2	1	0	6/8
	1/2	1/2	1/2	6/8
	1/2	1	1	10/8
H_o atoms	1/4	1/4	1/4	3/8
	3/4	1/4	1/4	5/8
	3/4	3/4	1/4	7/8
	3/4	3/4	3/4	9/8

written in the form of the coordinate of the fcc phase as

$$\begin{aligned} x_{hcp} &= \frac{1}{\sqrt{2}}x_{fcc} - \frac{1}{\sqrt{2}}y_{fcc}, \\ y_{hcp} &= \frac{1}{2\sqrt{2}}\frac{c_{hcp}}{a_{fcc}}x_{fcc} + \frac{1}{2\sqrt{2}}\frac{c_{hcp}}{a_{fcc}}y_{fcc} - \frac{2}{\sqrt{3}}\frac{a_{hcp}}{a_{fcc}}z_{fcc}, \\ z_{hcp} &= \sqrt{\frac{2}{3}}\frac{a_{hcp}}{a_{fcc}}x_{fcc} + \sqrt{\frac{2}{3}}\frac{a_{hcp}}{a_{fcc}}y_{fcc} + \frac{1}{2}\frac{c_{hcp}}{a_{fcc}}z_{fcc}. \end{aligned} \tag{4.7}$$

The Eq 4.7 can be tested by putting the coordinates of atoms on $(111)_f$ plane.

$$\begin{aligned} z_{hcp}(a_{fcc}, 0, 0) &= \sqrt{\frac{2}{3}}a_{hcp}, \\ z_{hcp}(0, a_{fcc}, 0) &= \sqrt{\frac{2}{3}}a_{hcp}, \\ z_{hcp}(0, 0, a_{fcc}) &= \frac{1}{2}c_{hcp}. \end{aligned} \tag{4.8}$$

The height of the three corner atoms should be the same on the hexagonal system, so the relation between a_{hcp} and c_{hcp} from Eq 4.2, can be expressed as

$$\begin{aligned} \sqrt{\frac{2}{3}}a_{hcp} &= \frac{1}{2}c_{hcp}, \\ \frac{c_{hcp}}{a_{hcp}} &= 1.63\,. \end{aligned} \tag{4.9}$$

For this reason, the c_{hcp}/a_{hcp} must be 1.63 to make the perfect fcc form in the hexagonal system. The last line of Eq 4.7 can be rewritten as

$$z_{hcp} = \frac{1}{2}\frac{c_{hcp}}{a_{fcc}}(x_{fcc} + y_{fcc} + z_{fcc}). \tag{4.10}$$

The positions of atoms which form the perfect fcc form in the hexagonal system can be calculated. They are showed in Table 4.1. It is noticed that the hydrogen

atoms are divided into eight fractions of c_{hcp}. The destination of hydrogen atoms will be monitered, so the path of hydrogen atoms which moves in the intermediate phase will be discussed in section4.5.

4.3 The structural phase transition

The theory in section 2.2 is used to find an energetically favorable phase at any pressure. The phase which has the lowest enthalpy under given pressure is energetically favorable. The structure of the hcp and the fcc phases are showed the Table 1.1. They are optimized every 5 GPa between $0-60$ GPa by the Geometry Optimization method. The calculations used two exchange-correlation energy, the LDA and the GGA. The enthalpies of the hcp and the fcc phases from our calculations are plotted with respect to the pressure as shown in Fig 4.5. The enthalpies

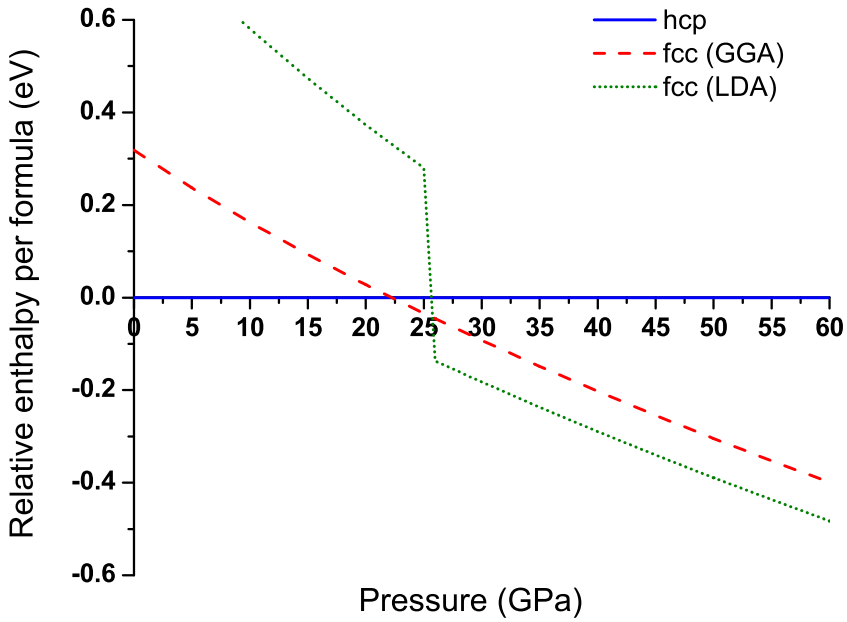

Figure 4.5: The enthalpy per formula is plotted with respect to the pressure. The enthalpy of the fcc phase with the GGA and the LDA calculations are plotted relative to the enthalpy of the hcp phase with the GGA and the LDA calculations, respectively. The blue line is the enthalpy of the hcp phase with both calculations. The red dash line is the enthalpy of the fcc phase with the GGA calculation. The green dot line is the enthalpy of the fcc phase with the LDA calculation.

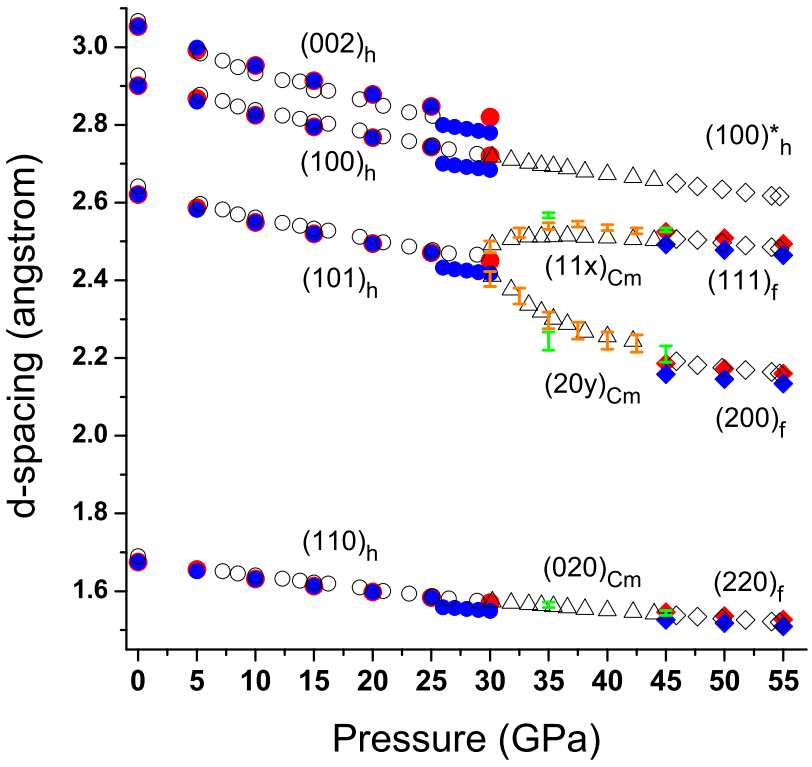

Figure 4.6: The d-spacing from the GGA calculation (red symbols), the LDA calculation (blue symbols) and the experimental results (opened symbols). The graphs are divided into three parts: the left part is the hcp phase (circles), the center is the intermediate phase (triangles), the right is the fcc phase (diamonds). The green bars are computed from the integer-indexing planes of the Cm structure. The orange bars are calculated from the non-integer indexing planes of the Cm structure. The bars contain the d-spacing values of the configurations of the $1^{st} - 5^{th}$ steps.

are plotted relative to that of the hcp phase. The graphs show that the hcp phase is more energetically favorable at low pressure and then the fcc phase becomes energetically favorable than the hcp phase at 26 and 22 GPa for the calculation with the LDA and the GGA, respectively. Both calculations give slightly low transition pressure which should be about 46 GPa. The 26 and 22 GPa transition pressure are closed to the hcp phase to intermediate phase transition which is at about 25 GPa from the IR experiment. For this reason, although the fcc phase is energetically favorable but it has not been observed by the experiment. The system transforms to the intermediate phase first. Therefore, the enthalpy of the intermediate phase which is not included in Fig 4.5 have to be lower than that of the fcc phase at pressure $<$ 46 GPa; however, the calculation of the intermediate phase discussed in section 3.5 shows that the enthalpy of intermediate phase is higher than of the hcp and the fcc phases, so it is plotted as the barrier that the system has to climb up sluggishly.

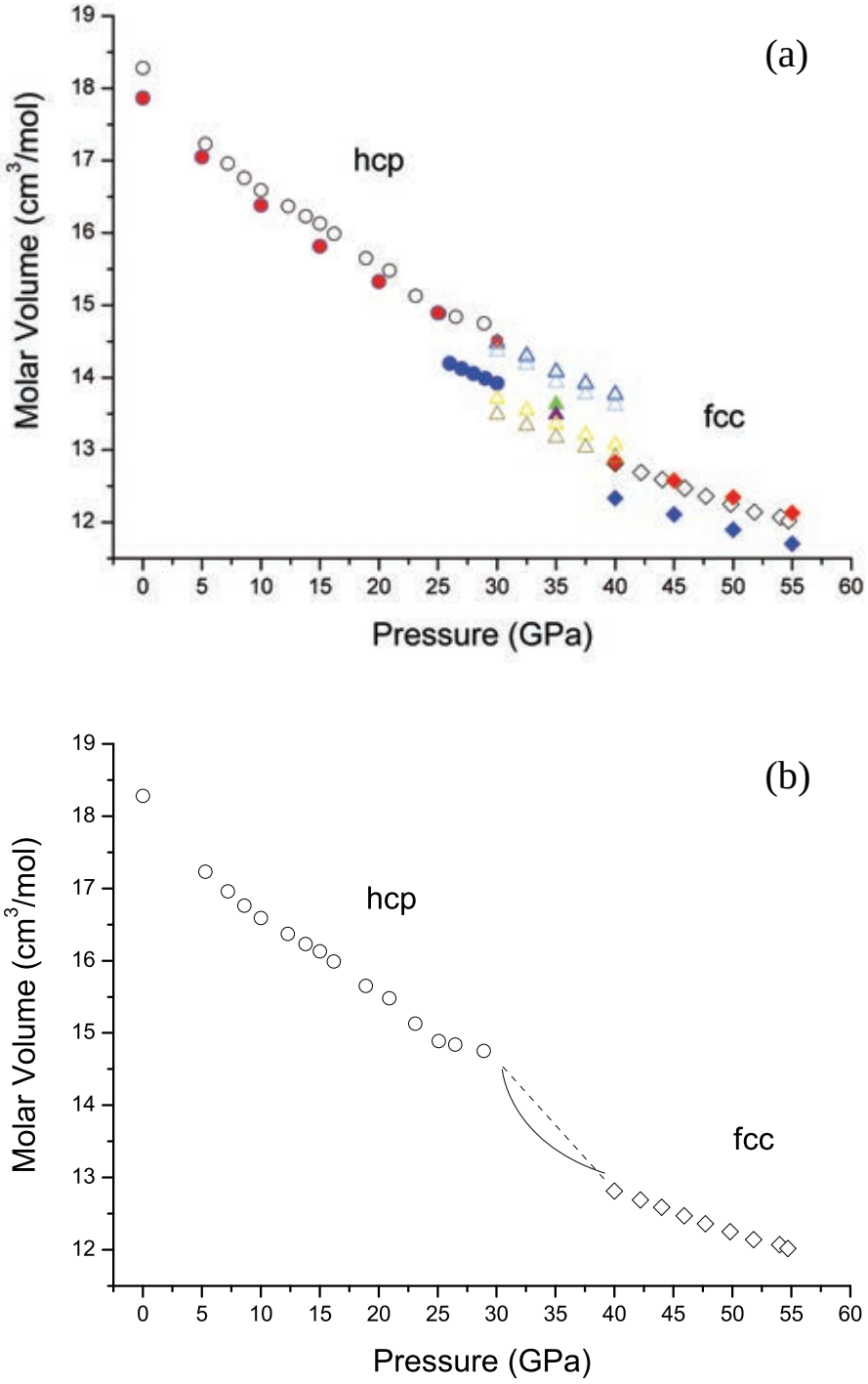

Figure 4.7: (a) The molar volume from the experiment (open symbols) compared with the GGA (red solid symbols) and the LDA (blue solid symbols) was calculations. It is divided into three parts; the circle is the hcp phase, the triangle is the intermediate phase and the diamond is the fcc phase. The open triangles are the $1^{st} - 5^{st}$ steps which are among the intermediate phase ordered from top to bottom. The solid triangles are the $(3 + 1/3)^{rd}$ and $(3 + 2/3)^{rd}$ steps that dominate the empty space between the molar volume of the hcp and the fcc phases. (b) The molar volume of the intermediate phase is predicted by the guessing lines which are dashed straight line and solid curve line.

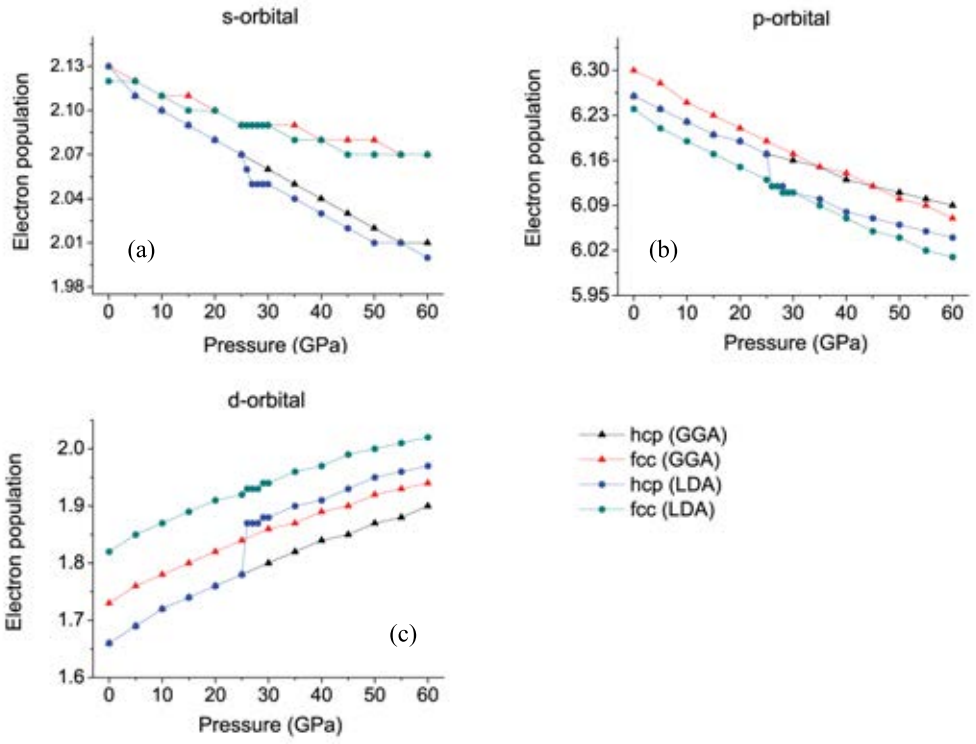

Figure 4.8: The graphs represent the electron population in each orbital as the pressure increases. The electron population of hcp and fcc phases which are in s orbital in figure (a), p orbital in figure (b) and d orbital in figure (c) are GGA and LDA calculations.

The lattice parameters can also be obtained from the calculations. They can be compared with those of the experiment in terms of the d-spacing and the molar volume. The d-spacing of $(002)_h$, $(110)_h$, $(101)_h$ and $(110)_h$ planes can be calculated from the equation of hexagonal system in Table 2.1. The d-spacing of $(111)_f$, $(200)_f$ and $(220)_f$ planes can be calculated from the equation of cubic system in Table 2.1. The d-spacing from the GGA calculation are plotted as the red symbols and in good agreement with the experimental d-spacing (open symbols) (see Fig 4.6). The molar volume is calculated by multiplying the Avogadro's number to the volume per formula. The molar volume from the GGA calculation is directly dependent on its d-spacing because they are both calculated from the lattice parameters. Therefore, it is plotted as the red symbols and in good agreement with the experiment (open symbols) (see Fig 4.7). The molar volume of the LDA calculation (the blue symbols) is associated with its d-spacing, too. They are in good agreement with the experiment at $0-25$ GPa but they underestimate compared with the experimental value at pressure ≥ 26 GPa. According to the Fig 4.5, the enthalpy from the LDA calculation decreases discretely at $25-26$ GPa.

This is an unnatural behavior for the first order phase transition. The

Mulliken population analysis* shows that the electron transfers from $4p \rightarrow 3d$ continuously as the pressure increases, but it transfers discontinuously at $25 - 26$ GPa (see Fig 4.8). It causes changing in the bonding between atoms. Moreover, this effect causes the atoms to get closer, i.e. the d-spacing and molar volume have large contracted values at $25 - 26$ GPa. These were not observed in experiment. Therefore, we conclude that the GGA calculation is more reliable than the LDA calculation. The barrier in the next section will be calculated by the GGA only.

4.4 The barrier

The barrier is the energy that obstructs the phase transition from hcp phase to fcc phase. Generally, the thermal effect which has the energy of 25 meV at room temperature can assist the structural transformation to cross the barrier. The paths of scandium and hydrogen atoms are divided into small steps by Eq 3.10. All atoms are fixed at each calculation step. The energy will be calculated and plotted with respect to the steps. The paths of scandium atoms are already discussed in section 4.1. From section 4.2, the initial and the final positions of hydrogen atoms are shown. At first thought, the hydrogen atoms might move in the shortest way and give us the lowest energy configuration. This is not the case. The track of hydrogen atoms is shown in Fig 4.9. The enthalpy of 6 steps which are the hcp phase, the $1^{st} - 5^{th}$ steps configurations and the fcc phase at the 6^{th} step is shown in Fig 4.10. The barrier is shown as the enthalpy as a function of the scaled displacement. The scaled displacement (μ) is the ratio of distance in $[1\bar{1}0]$ and $[\bar{1}10]$ directions that atoms move from the hcp phase to the fcc phase. The hcp phase is set at $\mu = 0$ and the fcc phase is set at $\mu = 1$. Therefore, $0 < \mu < 1$ is the intermediate phase. The enthalpies from DFT are plotted relatives to the enthalpy of the hcp phase. When μ is more than 0, the enthalpy is higher until highest at $\mu = 0.5$. The height of the barrier is 22 eV per formula at 25 GPa. It is about 880 times higher than of the room temperature effect, so this path cannot be used to describe the transformation from the hcp phase to the fcc phase. Because some hydrogen atoms will get too close to each other by this path that lead to the high energy.

Thus we resort to another path as follows; the scandium atoms are fixed but the hydrogen atoms are set to move freely to their equilibrium in each step. The barrier is calculated more precisely with 18 finer steps i.e. by dividing the hcp

*See Appendix E

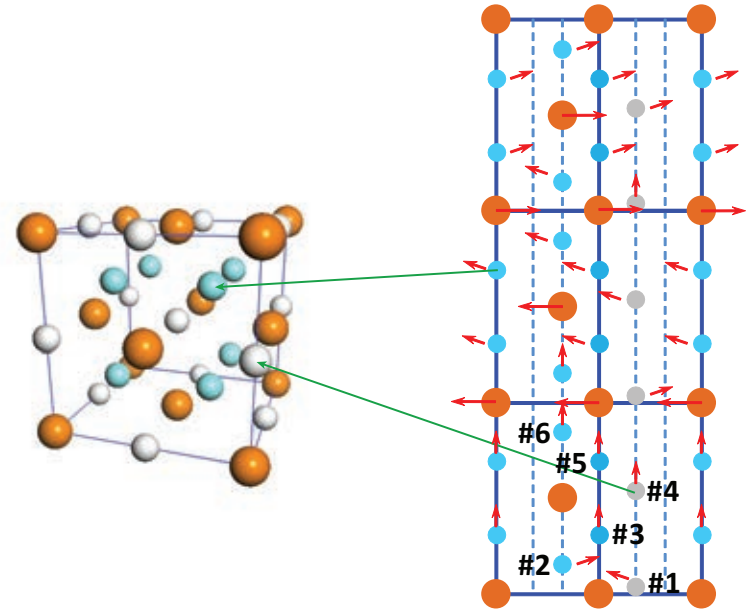

Figure 4.9: The hydrogen tracks are guessed that they move in the shortest way. The blue hydrogen atoms in hcp phase should be replaced the blue hydrogen atoms in fcc phase. The white one is also. (Noting that this guessing is failure.)

-6^{th} steps by three. Fig 4.11, the solid symbols label the normal hcp -6^{th} steps and the open symbols label the others finer step. The enthalpies are a bit lower at $\mu > 0$ and raise up until the highest at $\mu = 0.56$. The height of barrier which is 0.41, 0.37, 0.32 eV per formula at 25, 35, 45 GPa, respectively, reduces a lot from the previous compare (compare Fig 4.10 and Fig 4.11). Even though the barrier is still higher than the room temperature effect. From the enthalpy per atom, the barriers are 0.10, 0.09, 0.08 eV per atom at 25, 35, 45 GPa, respectively. They are only about four times of the room temperature effect. However, which energy that the structure gain to drive the transformation? This question will be discuss at the end of this chapter. Moreover, the transformation cannot reach to the fcc phase easier because the barrier decreases only slightly as the pressure increases. It may cause the transformation under wide range of pressure.

The c/a is calculated as shown in Fig 4.12. The result can be divided into two parts. The first part is the $1^{st} - 3^{rd}$ steps which have the c/a of about $1.76 - 1.77$. They can be viewed as a distorted-hcp. The c/a drops significantly at $(3 + 1/3)^{rd}$ step or $\mu = 0.56$ of which the enthalpy is the top of the barrier. The second part has the c/a of about $1.64 - 1.65$ at the $4^{th} - 5^{th}$ steps. The c/a converges to 1.63 at the 6^{th} step that is the ratio for the perfect fcc form, then the second part can be viewed as a distorted-fcc. Therefore, the structure of the left side of the barrier is the distorted-hcp and the structure of the right side of the barrier is the distorted-fcc. In another word, the distortion of structure which becomes the

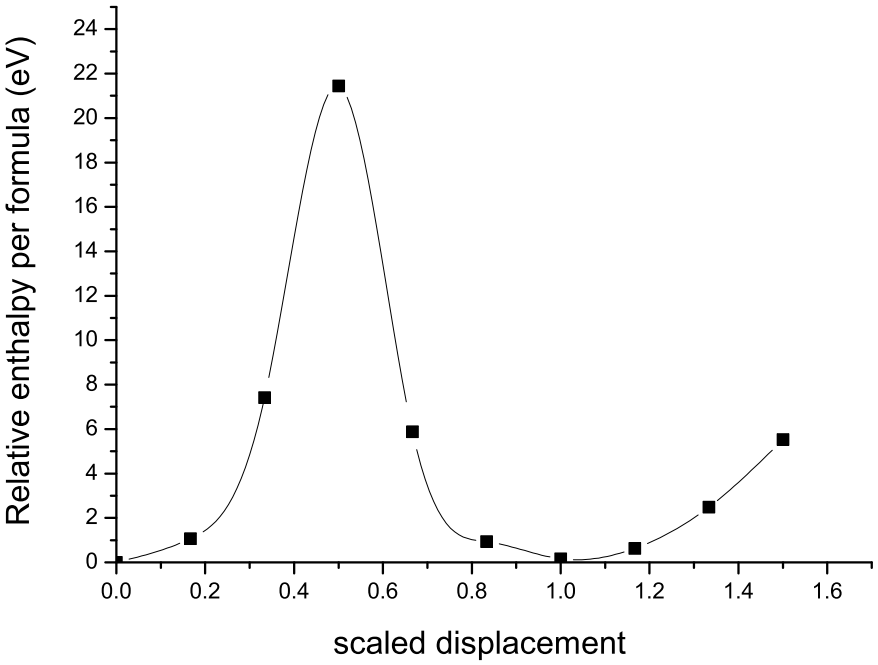

Figure 4.10: The barrier of the guessing hydrogen path at 25 GPa is illustrated. It is plotted relative to the enthalpy of the hcp phase. $\mu = 0$ is the atoms in the hcp positions and $\mu = 1$ is the atoms in the fcc positions.

distorted-hcp gives the higher enthalpy until the distortion of structure reaches $\mu = 0.56$ or becomes distorted-fcc, then the enthalpy is lowered. The d-spacing of intermediate phase can be calculated from the equation of the monoclinic system in Table 2.1. From section 3.1, the intermediate phase which is the Cm phase has three d-spacing which are in the monoclinic system. The d5 plane is neither $(112)_{Cm}$ plane nor $(111)_{Cm}$ plane. It is occurred by the dispersion of the $(112)_{Cm}$ to $(111)_{Cm}$ plane, so the plane indices should not be integer. The decimal x runs from 2 to 1 in $(11x)_{Cm}$ plane. This is called non-integer indexing plane. In another word, it is a very standing contained in a larger unit cell. In Fig 4.6, the d-spacing of $(11x)_{Cm}$ plane, shown in Table 4.1, matches with the d5 plane very well. The non-integer indexing plane is really the integer indexing plane of a larger supercell of Cm phase. The supercell is $n \times n \times n$ unit cell, when n is the value that can multiply x to be an integer. For example, $x = 1.5$ is multiplied by 2 to be an integer so the $(11x)_{Cm}$ plane with $x = 1.5$ is the $(223)_{Cm}$ plane in $2 \times 2 \times 2$ unit cell. The d6 plane is neither $(201)_{Cm}$ plane nor $(202)_{Cm}$ plane, also. The decimal y runs from 1 to 2 in $(20y)_{Cm}$, shown in Table 4.2. It can explain the d6 plane very well, too. The last plane is the d7 plane. Using $(020)_{Cm}$ plane to represent the d7

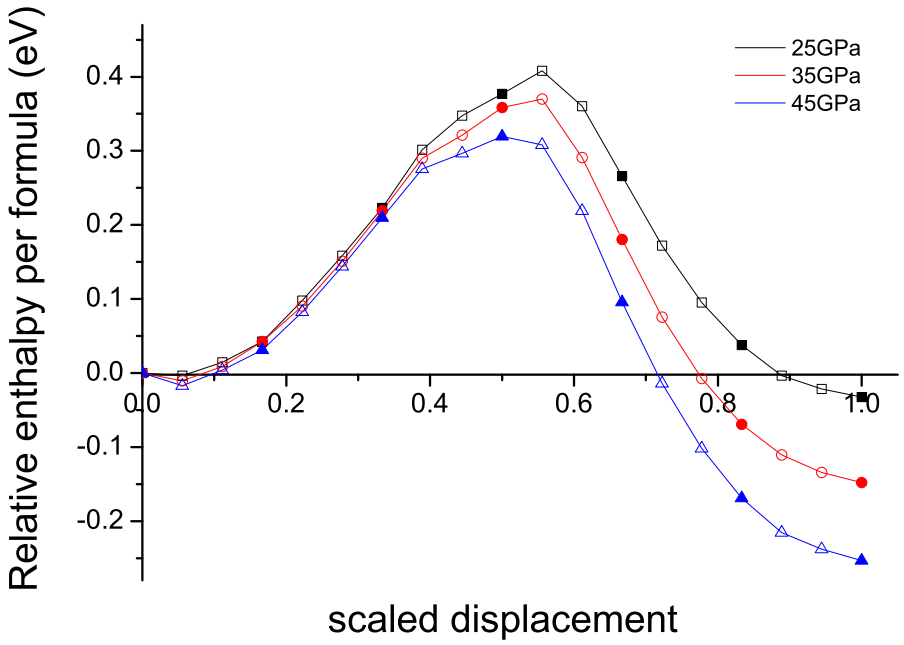

Figure 4.11: The barriers are shown for the pressure at 25 (black), 35 (red) and 45 (blue) GPa. They are plotted relative to the enthalpy of the hcp phase at each pressure. $\mu = 0$ is the atoms in the hcp positions and $\mu = 1$ is the atoms in the fcc positions. The solid symbols are the hcp-6^{th} steps. The open symbols are the finer steps.

plane in the d-spacing calculation give good agreement with the experiment.

Fig 4.7 shows the molar volume of the hcp and the fcc phases of which the calculations are in good agreement with experiment. The molar volume of the fcc phase is discontinuous from that of the hcp phase, so the molar volume of the intermediate phase must be the link between them. The molar volumes of the $1^{st} - 3^{rd}$ steps are similar to the molar volume of the hcp phase. The molar volumes of the $4^{th} - 5^{th}$ steps are similar to the molar volume of the fcc phase. Therefore, the molar volume of the intermediate phase is between of the $3^{rd} - 4^{th}$ steps. This is the period of the transformation from the distorted-hcp to the distorted-fcc analyzed from the c/a. The molar volume of the intermediate phase with respect to the pressure can possibly be a straight line or a curve line, but there is not enough information from experiment for discussion, so we left it for the new information in the future.

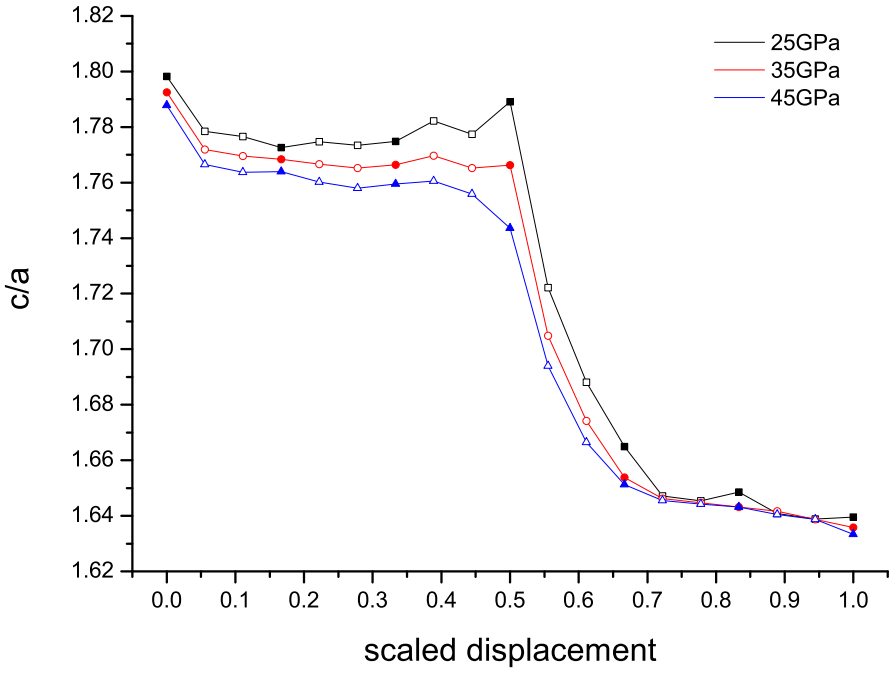

Figure 4.12: The c/a is represented at 25 (black), 35 (red) and 45 (blue) GPa. The scaled displacement equals to 0 is the hcp and 1 is the fcc. The hcp-3^{rd} steps show that the c/a are about $1.74 - 1.80$. The $4^{th} - 6^{th}$ steps shows that the c/a drop to $1.63 - 1.66$.

4.5 Path of hydrogen atoms

The motion of the atoms of the intermediate phase is shown in Fig 4.13 and Fig 4.14. The scandium atoms are fixed along the path from the hcp phase to the fcc phase and then the hydrogen atoms are relaxed to find their position with (local) minimum energy. The steps are ordered by sort ascending from the ligther to the darker colored atoms. The forward steps are the intermediate phase as the pressure increases. At the initial position, the hydrogen atoms near T site of the hcp phase are grey and blue atoms and near M site of the hcp phase are red atoms. The grey atoms move to the T site of the fcc phase at the final position. The tracks of the blue and the red atoms are divided into two parts which are the upper half and the lower half of hexagonal unit cell. At the upper half, the blue atoms move to the O site of the fcc phase and the red atoms move to the T site of fcc phase at the final position. At the lower half, the paths of the blue and the red atoms switch each other between the 3^{rd} and 4^{th} steps. The red atoms move to higher than the blue atoms and stay on the O site at the final position. The blue atoms move to lower than the red atoms and stay on the T site at the final position. The switching site with crossing paths of the blue and the red atoms can

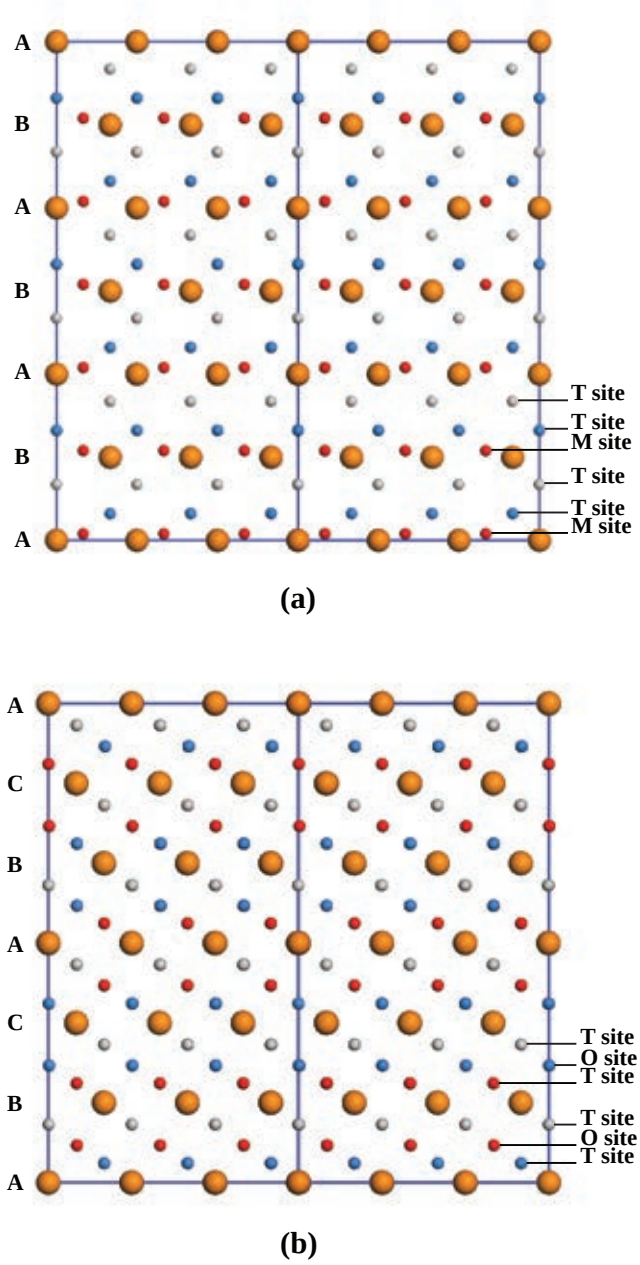

Figure 4.13: The figures show atomic movement tracks during the hcp to fcc transition. The Sc atoms are in orange and the H atoms are in red, blue, and grey. These tracks are the projection of the PR configuration onto the $(110)_h$ planes. (a) The starting point is the hcp. (b) The 6^{th} step is the fcc. The stacking planes are labeled by standard notation A, B and C. The symmetry sites (T and M sites of the hcp, and T and O sites of the fcc) are indicated for references.

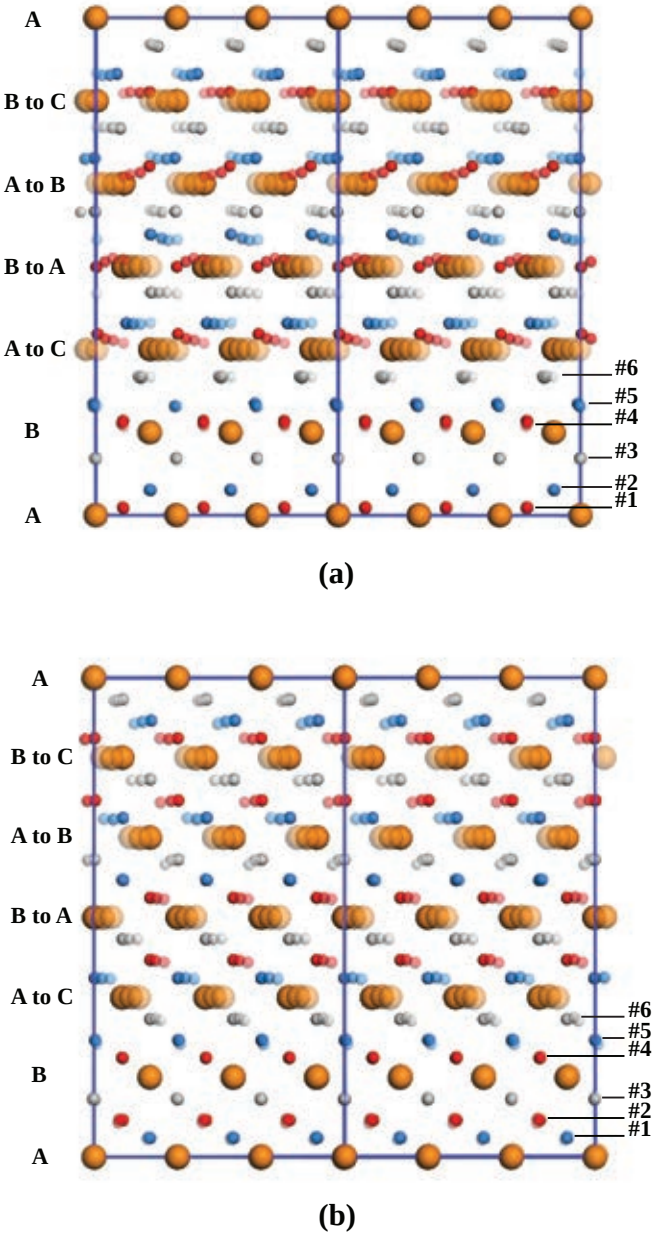

Figure 4.14: The figures show atomic movement tracks during the hcp to fcc transition. The Sc atoms are in orange and the H atoms are in red, blue, and grey. These tracks are the projection of the PR configuration onto the $(110)_h$ planes. (a) The atomic tracks from the hcp to the 3^{rd} step. (b) The atomic tracks of the $4^{th} - 6^{th}$ steps. The lighter colors labeled the earlier steps. The stacking planes are labeled by standard notation A, B and C. The numbered labels are indicated for references.

Table 4.2: The non-integer index of the newly forming planes $(11x)_{Cm}$ and $(20y)_{Cm}$ at various pressure.

Pressure (GPa)	x in $(11x)_{Cm}$	y in $(20y)_{Cm}$
25.0	2	1
30.0	1.7	1.2
32.5	1.4	1.4
35.0	1.2	1.7
37.5	1.1	1.8
40.0	1.1	1.9
42.5	1.1	1.9
45.0	1	2

be matched to the dropping of the c/a that is the structural transformation from the distorted-hcp to the distorted-fcc. The Raman experiment of the hcp phase shows the Raman-active O_v modes around 500 cm^{-1} [6]. It means that there is no any hydrogen atoms stay on the O sties. However, the Raman experiment of the intermediate phase shows this peak is broadening. This result matches to our result that some hydrogen atoms move slowly to the O site. The hydrogen atoms on the O site cause the O_v modes inactive and the peak broadening.

Moreover, there is the difference in bonding between scandium and hydrogen atoms on each site. The labeling number due to the order of hydrogen atoms in Fig 4.15a which No. 1 & 4 are near M site, and No. 2, 3, 5 & 6 are near T site. The Mulliken population analysis shows the charges (Mulliken charges) of the atoms. The hydrogen atoms in hcp phase at 35 GPa have -0.34 charges near T site and -0.31 charges near M site (see Fig 4.15b). The scandium atom has +0.99 charges. The hydrogen atoms bond strongly to the scandium atoms which they surround, and bond weakly with anti-bonding to the scandium atoms which they do not surround (see Fig 4.16a,b). When the structure transforms from the distorted-hcp to the distorted-fcc at the $3^{rd}-4^{th}$ steps, the nature of charge and bonding change, too. The hydrogen atoms No. 1 & 5 are at O site and No. $2-4$ & 6 are at T site. The hydrogen atoms in the fcc phase have -0.22 charges near O site and -0.33 charges near T site (see Fig 4.15b). The scandium atom has +0.89 charges. The hydrogen atoms at T site bonds strongly to the scandium atom which it surrounds as before. Nevertheless, the hydrogen atom at O site bonds to both of scandium atoms which surround it equally. The hydrogen pair distribution is also plotted

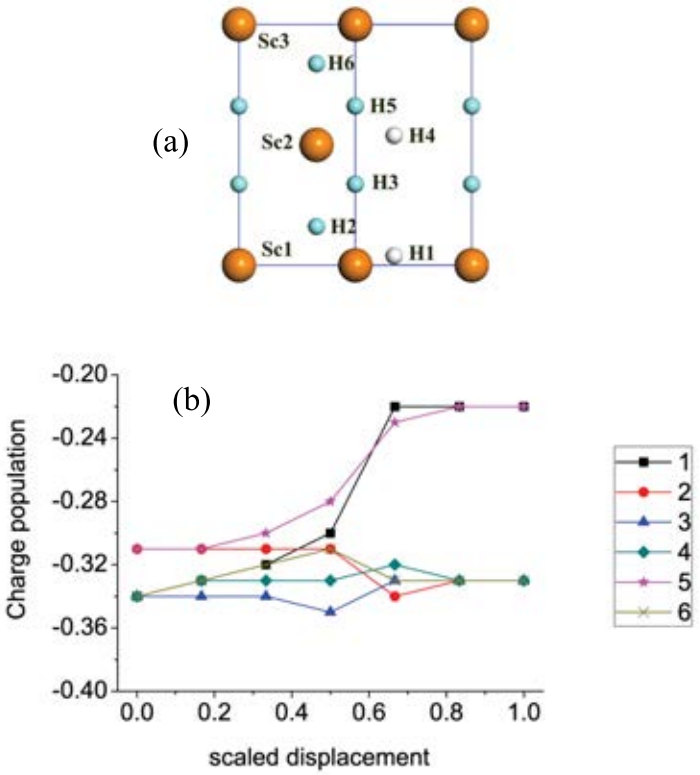

Figure 4.15: (a) The scandium and hydrogen atoms are labeled to separate their positions by the numbers. (b) The charge population and (c) the bonding population between each hydrogen atom and a scandium atom are plotted where the black, red and blue lines are the scandium atoms number 1, 2 and 3, respectively. The numbers are being owned by hydrogen and scandium atoms with labeling in (a).

(see Fig 4.17 and Fig 4.18). The first peak of the hcp phase at 35 GPa is very broad and centered around $1.80 - 2.15$ Å. It disperses when the metal plane slides out of the ABABAB pattern and forms into two separate peaks in the fcc phase at around $1.90 - 1.95$ Å and $2.20 - 2.25$ Å. It dues to the "blocking effect". The previous theoretical study showed that two hydrogen atoms in metal hydrides are in equilibrium when their interval is about 2 Å [20, 21].

4.6 Discussion on high barrier value

There are two hypothesises about the high barrier value that could be examined in the future work. First, there is the coexist phase between dihydride and trihydride. The dihydride is the fcc phase. The experiment [3] showed that the coexist phase exists until the trihydride transform into the fcc phase at 46 GPa. The difference of the stacking sequence between ABCABC of dihydride and ABABAB of trihydride

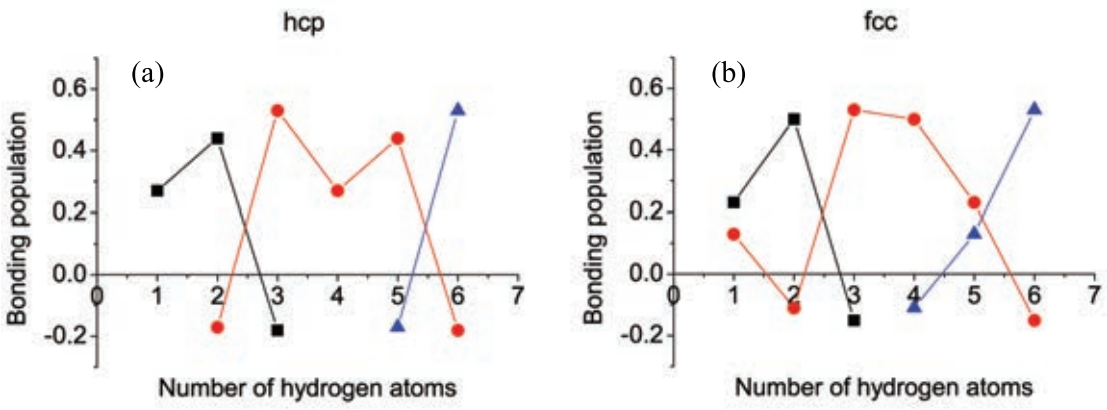

Figure 4.16: The bonding population between each hydrogen atom and a scandium atom are plotted where the black, red and blue lines are the scandium atoms number 1, 2 and 3, respectively. (a) is of the hcp phase and (b) is of the fcc phase. The numbers are being owned by hydrogen and scandium atoms with labeling in Fig 4.15a.

may effect the high energy at the phase boundary[†]. This energy lower barrier. The structure near phase boundary transforms to the fcc phase first and then the phase boundary expands until the whole bulk. Therefore, the trihydride that prefers to be the fcc phase since 22 GPa (this work) and the energy at phase boundary may drive the intermediate phase cross the barrier.

Second, the neutron diffraction experiment showed that the thermal factors[‡] (B factor) of the hydrogen atom in Table 1.1 are very high [4]. The H_t and H_m atoms have the B factor = 2.40 and 1.50 Å^2, respectively, while the scandium atom has the B factor = 0.46 Å^2. The high B factors of the hydrogen atom are much higher than that of the scandium atom, so the scandium atom see that the hydrogen atoms has dynamical movement as an atomic distribution around it. However, this work calculated the system in the fixed basis case, so some information of dynamical movement may be concealed.

[†]The boundary between the fcc phase of dihydride and the hcp phase of trihydride.
[‡]See Appendix A

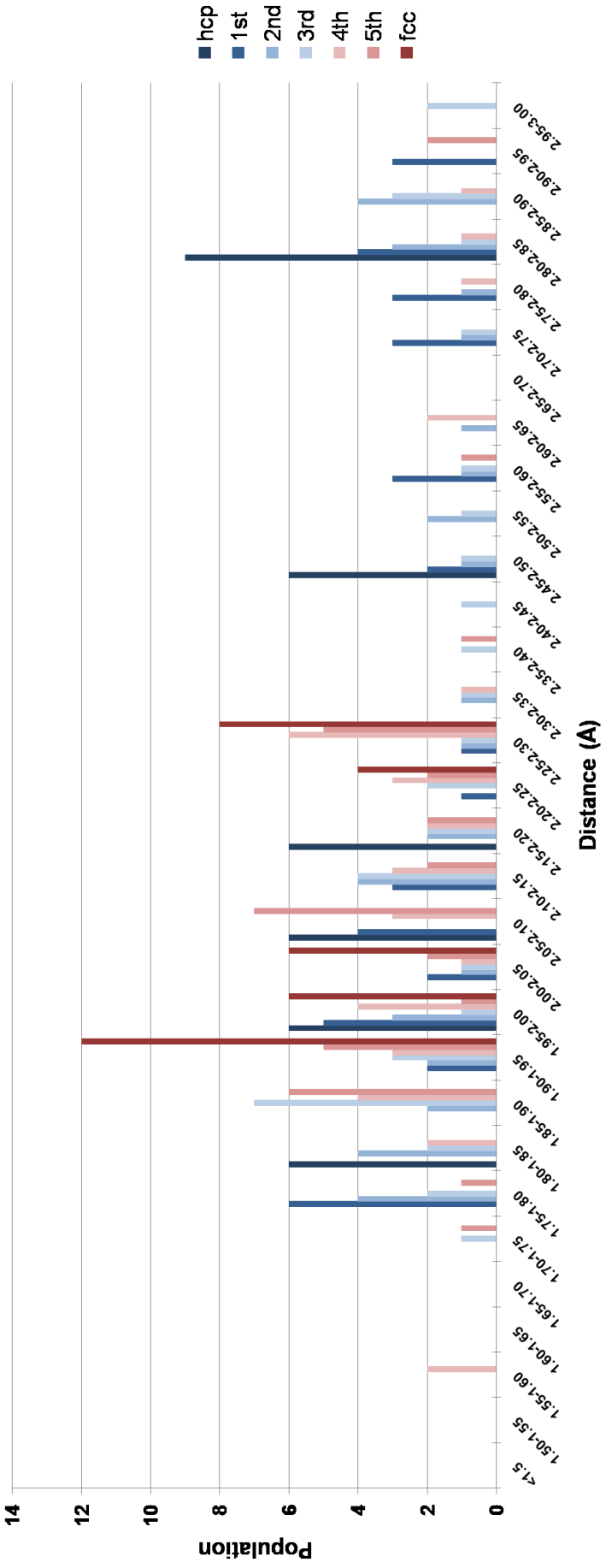

Figure 4.17: The figure shows the radial distribution between hydrogen-hydrogen atoms at 25 GPa.

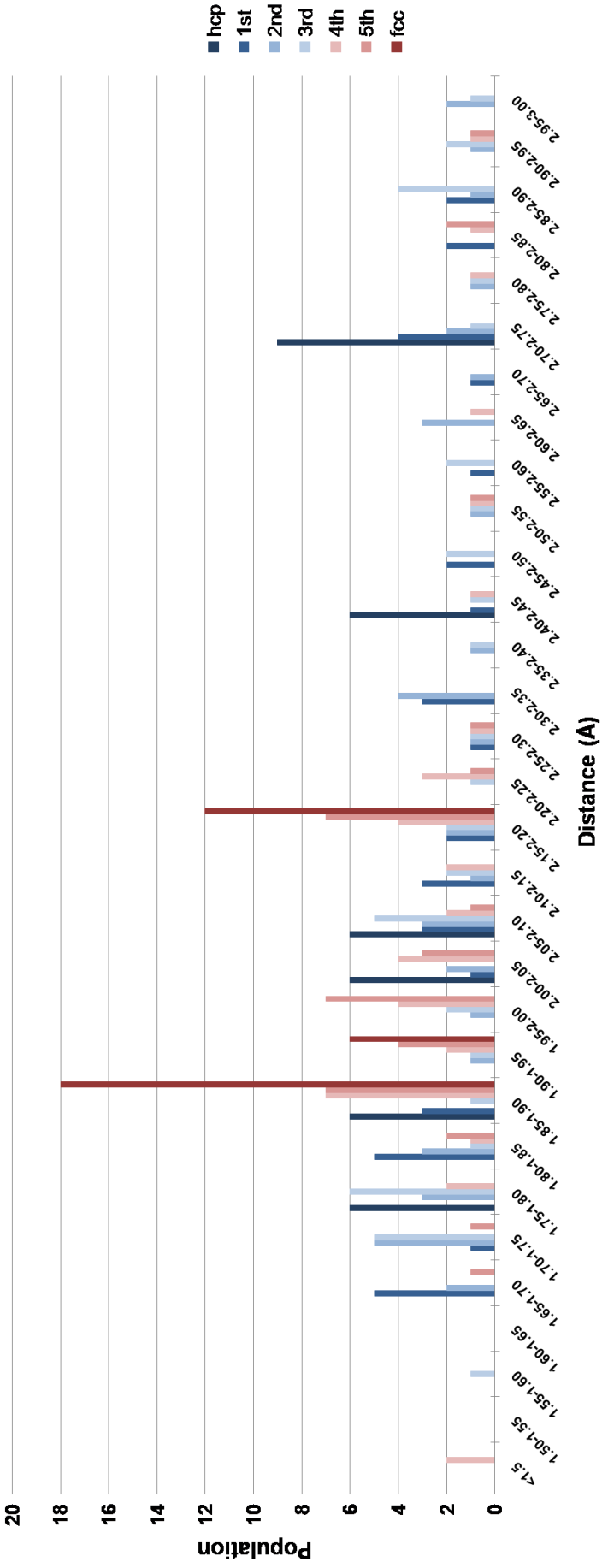

Figure 4.18: The figure shows the radial distribution between hydrogen-hydrogen atoms at 45 GPa.

Chapter V

CONCLUSIONS

The structural phase transition of ScH_3 was studied by using DFT. In the calculation, we considered two phases which are the hcp and the fcc phases. The results showed that the hcp phase is more energetically favorable at ambient pressure, and the fcc phases is more energetically favorable at 22 GPa and 26 GPa in GGA and LDA calculations, respectively. The transition pressures are contrast to the experimental result of 46 GPa therefore the intermediate phase must be taken into account.

The intermediate phase is the phase which occur during the transformation from the hcp phase to the fcc phase. The stacking sequence of the scandium planes changes from ABABAB to ABCABC pattern on the $(110)_h$ planes. The AB sequence changes to CA sequence in $[1\bar{1}0]_h$ direction and the another AB sequence changes to BC sequence in $[\bar{1}10]_h$ direction. The calculation was separated into 6 steps and 18 finer steps by dividing the moving distance. The moving distance is shown as the scale displacement (μ) which $\mu = 0$ is the hcp phase and $\mu = 1$ is the fcc phase. The calculation of the intermediate phase used the GGA functional only. Because the d-spacing and the molar volume of the hcp phase for LDA calculation decrease drastically when the pressure increases from 25 to 26 GPa. The evidence is contrast to of the experimental results. Therefore, the calculation with GGA is more reliable than that with LDA. The structures of each step were optimized by fixing the positions of scandium atom and relaxing the positions of hydrogen atoms. The barrier decreases sluggishly as the pressure increases. The heights of the barrier are 0.41, 0.37, 0.32 eV for 25, 35, 45 GPa, respectively.

The structural analysis shows that the intermediate phase has the Cm symmetry. We pointed out this problem for the first time in literature [22]. The $(110)_h$ plane and the $(220)_f$ plane is equivalent to the $(020)_{Cm}$ plane. The $(101)_h$ plane is equivalent to the $(112)_{Cm}$ plane. It transforms to the $(111)_{Cm}$ plane which is equivalent to the $(111)_f$ plane. The $(1\bar{1}0)_h$ plane has the d-spacing equivalent to the $(101)_h$ plane, so it vanishes from the experimental result. The $(1\bar{1}0)_h$ plane is equivalent to the $(201)_{Cm}$ plane. It transforms to the $(202)_{Cm}$ plane which is equivalent to the $(200)_f$ plane. However, among the transformation the indices

of the plane are non-integer. The $(112)_{Cm}$ plane transforms to the $(111)_{Cm}$ plane by passing through the $(11x)_{Cm}$ plane at the intermediate phase. The $(202)_{Cm}$ plane transforms to the $(201)_{Cm}$ plane by passing through the $(20y)_{Cm}$ plane at the intermediate phase. The calculations of the d-spacing of the $(11x)_{Cm}$ and the $(22y)_{Cm}$ planes are good in comparison to the experimental result.

The hydrogen behavior is shown after the hydrogen atoms were relaxed. They can be divided into three kinds of their positions; the M site, the T site and the O site according to the symmetry points. There is the site switching between the $3^{rd} - 4^{th}$ steps which dues to the reduction of the c/a ratio from ~ 1.75 to ~ 1.63. The site switching can be divided into two sections; the lower half and the upper half of the hexagonal unit cell. At the lower half, the hydrogen atoms at M and T sites of the hcp phase move to O and T sites of the fcc phase, respectively. At the upper half, the hydrogen atoms at M and T sites of the hcp phase move to T and O sites of the fcc phase, respectively. The others two hydrogen atoms at T sites of the hcp phase move to T sties of the fcc phase. From Raman experiment [6], the hydrogen atoms arrange themselves in some distribution due to the broadening Raman peaks around 500 cm^{-1}. The charges of the hydrogen and the scandium atoms in hcp phase are ~ -0.33 and $\sim +0.99$ charges, respectively, at 35 GPa. The charges of the H_o and the H_t atoms in hcp phase are ~ -0.22 and $\sim +0.33$ charges, respectively, while the charges of the scandium atoms are $\sim +0.89$ charges at 35 GPa. This behavior dues to radial distribution of the distance between H-H atoms. It shows that the hydrogen atoms, which distribute equally around $1.80 - 2.00$ Å in the hcp phase, separate to be two peaks around $1.85 - 1.90$ and $2.15 - 2.20$ Å in the fcc phase at 45 GPa. The distances between H-H atoms are about 2.00 Å which dues to the "blocking effect" from the previous theoretical study [20, 21]. The hydrogen atoms were fixed while the scandium atoms were moved with the wide and short distances.

However, the barrier is too high for the structure to transform from the hcp phase to the fcc phase by the thermal energy alone. There are two hypothesises for this finding. First, the energy between the coexist phase; the dihydride and trihydride, that make the higher energy of the hcp phase. Second, the experiment found that the hydrogen atoms distribute widely around the scandium atoms but our calculations which is the static calculation may neglect this dynamical result. On the other hand, the intermediate phase are well explained by the mechanism of transformation which pass through the Cm symmetry and the hydrogen behavior is in good agreement with to the previous studies.

REFERENCES

[1] Griessen R, Huiberts JN, Kremers M, van Gogh ATM, Koeman NJ, Dekker JP and Notten PHL. Yttrium and lanthanum hydride films with switchable optical properties. **J. Alloys Comp.** 253-254 (1997) : 44-50.

[2] Kim DY, Scheicher RH, Mao H, Kang TW and Ahuja R. General trend for pressurized superconducting hydrogen-dense materials. **Proc. Natl. Acad. Sci. USA** 107 (December 2010) : 2793-2796.

[3] Ohmura A, Machida A, Watanuki T, Aoki K and Nakano S and Takemura K. Pressure-induced structural change from hexagonal to fcc metal lattice in scandium trihydride. **J. Alloys Compd.** 446 (April 2007) : 598.

[4] Antonov VE, Bashkin IO, Fedotov VK, Khasanov SS, Hansen T, Ivanov AS, Kolesnikov AI and Natkaniec I. Crystal structure and lattice dynamics of high-pressure scandium trihydride. **Phys. Rev. B** 73 (February 2006) : 054107.

[5] Machida A, Ohmura A, Watanuki T, Ikeda T, Aoki L, Nakano S and Takemura K. X-ray diffraction investigation of the hexagonal-fcc structural transition in yttrium trihydride under hydrostatic pressure. **Solid State Commun.** 138 (May 2006) : 436-40.

[6] Kume T, Ohura H, Takeichi T, Ohmura, Machida A, Watanuki T, Aoki K, Sasaki S, Shimizu H and Takemura K. High-pressure study of ScH_3: Raman, infrared, and visible absorption spectroscopy. **Phys. Rev. B** 84 (August 2011) : 064132.

[7] Hohenberg P and Kohn W. Inhomogenous Electron Gas. **Phys. Rev.** 136 (June 1964) : B864.

[8] Kohn W and Sham LJ, Phys. Rev. 1965; 140:A1133.

[9] Herring C. A New Method for Calculating Wave Functions in Crystals. **Phys. Rev.** 57 (June 1940) : 1169-77.

[10] Phillips J and Kleinman L. New Method for Calculating Wave Functions in Crystals and Molecules. **Phys. Rev.** 116 (October 1959) : 287-94.

[11] Hamann DR, Schlüter M and Chiang C. Norm-Conserving Pseudopotentials. **Phys. Rev. Lett.** 43 (November 1979) : 1495-97.

[12] Vanderbilt D. Soft self-consistent pseudopotentials in a generalized eigenvalue formalism. **Phys. Rev. B** 41 (April 1990) : 7892-95.

[13] Ceperley DM and Alder BJ. Ground State of the Electron Gas by a Stochastic Method. **Phys. Rev. Lett.** 45 (April 1980) : 556.

[14] Perdew JP and Zunger A. Self-interaction correction to density-functional approximations for many-electron systems. **Phys. Rev. B** 23 (May 1981) : 5048-5079.

[15] Perdew JP, Burke K and Ernzerhof M. Generalized Gradient Approximation Made Simple. **Phys. Rev. Lett.** 77 (October 1996) : 3865.

[16] Clark SJ, Segall MD, Pickard CJ, Hasnip PJ, Probert MIJ, Refson K and Payne MC. First principles methods using CASTEP. **Z. Kristallogr.** 220 (June 2005) : 567-70.

[17] Monkhorst HJ and Pack JD. Special points for Brillouin-zone integrations. **Phys. Rev. B** 13 (June 1976) : 5188-5192.

[18] Monkhorst HJ and Pack JD. "Special points for Brillouin-zone integrations" - a reply. **Phys. Rev. B** 16 (August 1977) : 1748-1749.

[19] Pfrommer BG, Côté M, Louie SG and Cohen ML. Relaxation of Crystals with the Quasi-Newton Method. **J. Comput. Phys.** 131 (1997) : 233-40.

[20] Switendick AC. Band Structure Calculations for Metal Hydrogen Systems. **Z. Phys. Chem.** 117 (March 1979) : 89-112.

[21] Rao BK and Jena P. Switendick criterion for stable hydrides. **Phys. Rev. B** 31 (May 1985) : 6726-6730

[22] Pakornchote T, Pinsook U and Bovornratanaraks T. The hcp to fcc transformation path of scandium trihydride under high pressure. **J. Phys. Condens. Matter** 26 (January 2014) : 025405.

[23] Parr RG and Yang W. **Density-funtional theory of atoms and molecules**. New York: Oxford University Press, 1989.

[24] Sanchez-Portal D, Artacho E and Soler JM. Projection of plane-wave calculations into atomic orbitals. **Solid State Commun.** 95 (May 1995) : 685-690.

[25] Mulliken RS. Electronic population analysis on LCAO-MO molecular wave functions. **J. Chem. Phys.** 23 (January 1955) : 1833-1846.

[26] Segall MD, Pickard CJ, Shah R and Pyne MC. Population analysis in plane wave electronic structure calculations. **Mol. Phys.** 89 (February 1996) : 571-577.

[27] Segall MD, Shah R, Pickard CJ and Pyne MC. Population analysis of plane-wave electronic structure calculations of bulk materials. **Phys. Rev. B** 54 (December 1996) : 16317-16320

APPENDICES

APPENDIX A

Structure factor

The x-ray has the wavelength in the order of Å which is the same order as the unit cell of the crystal. FIG A.1(a) shows that the x-ray beams are reflected by the atoms on the planes with 2θ with respect to the incident direction when the θ is the Bragg's angle. The x-ray beams are interference in the further length by considering the path difference (P.D.). The incident waves in direction $\mathbf{s}_0$ come to two atoms at difference planes and they were scattered by atoms in direction $\mathbf{s}$. Two reflected waves interfere in the further length and they will be constructive or destructive that depend on the Bragg's law in the Eq 2.2 and the P.D. is

$$\text{P.D.} = \text{AB} - \text{CD} = \mathbf{r}_1 \cdot \mathbf{s} - \mathbf{r}_1 \cdot \mathbf{s}_0 = \mathbf{r}_1 \cdot (\mathbf{s} - \mathbf{s}_0), \tag{A.1}$$

where $\mathbf{r}_1 = x_1\mathbf{a} + y_1\mathbf{b} + z_1\mathbf{c}$ is the position vector which points the atom in the unit cell. The direction of $(\mathbf{s} - \mathbf{s}_0)$ which is shown in Fig A.1(a) is parallel to the reciprocal space vector $\mathbf{G}_{hkl}$ and its modulus is equal to $2\sin\theta$. The $|\mathbf{G}_{hkl}|^2$ is $1/d^2$, so the Bragg's law can be modified to

$$\mathbf{s} - \mathbf{s}_0 = \lambda\mathbf{G}_{hkl}, \tag{A.2}$$

where n is omitted into $\mathbf{G}_{hkl}$. By adding the Eq A.2 into the Eq A.1 then

$$\text{P.D.} = \lambda(\mathbf{r} \cdot \mathbf{G}_{hkl}) = \lambda(hx_1 + ky_1 + lz_1). \tag{A.3}$$

The phase angle between two reflected waves is

$$\phi = \frac{2\pi}{\lambda} \times \text{P.D.} = 2\pi(hx_1 + ky_1 + lz_1). \tag{A.4}$$

The atomic form factor, f, is a measure of the scattering amplitude of an isolated atom. It can be drawn as the vector with the angle ϕ with respect to the horizontal line. The structure factor is the sum of the atomic form factor vector in the unit cell as be shown graphically in Fig A.2. For convenience, it can be written in the complex form as

$$F_{hkl} = \sum_{n=0}^{N} f_n e^{2\pi i(hx_n + ky_n + lz_n)}, \tag{A.5}$$

where the unit cell has N atoms with each atom is labeled the n^{th} atom. The

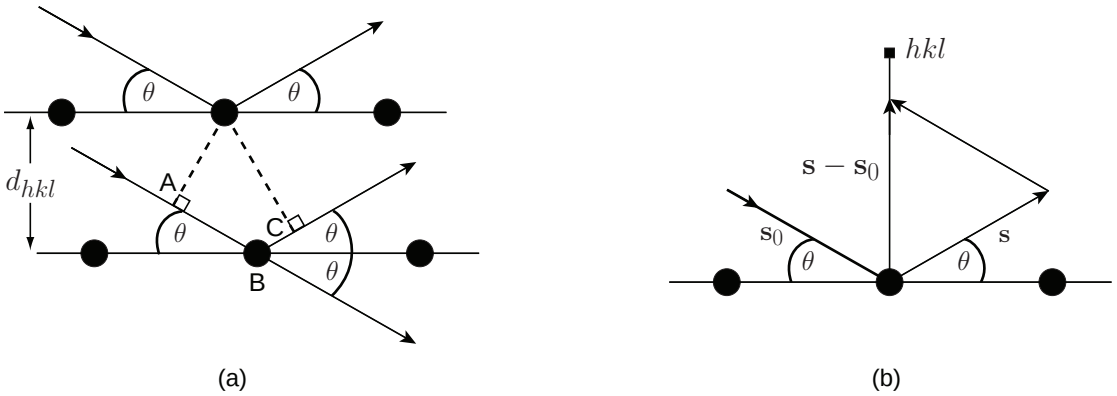

Figure A.1: (a) shows the x-ray diffraction of two planes. The reflected wave make the angle 2θ to the transmitted wave. (b) shows the resultant vector of the incident wave and the reflected wave is parallel to the reciprocal space vector.

structure factor of the neutron diffraction is slightly difference from of the x-ray diffraction by the scattering power

$$F_{hkl} = \sum_{n=0}^{N} b_n e^{-\frac{1}{2}\langle(\mathbf{G}\cdot\mathbf{u})^2\rangle} e^{2\pi i(hx_n+ky_n+lz_n)}, \tag{A.6}$$

where b is the scattering length and $\mathbf{u}$ is the displacement from the equilibrium point of the nucleus. The additional exponential term is the Debye-Waller factor or the thermal factor. The nucleus oscillate around the equilibrium point while the neutron come to scatter. The neutron beam is scattered from difference position of the same nucleus respect to time, so the measurement will measure the position of the nucleus by averaging over the time, $\langle \ldots \rangle$. In the experiment, the measurement is the intensity which is the modulus of the structure factor

$$I_{hkl} = |F_{hkl}|^2. \tag{A.7}$$

The intensity is used in the analysis the structure of the crystal by the above equations.

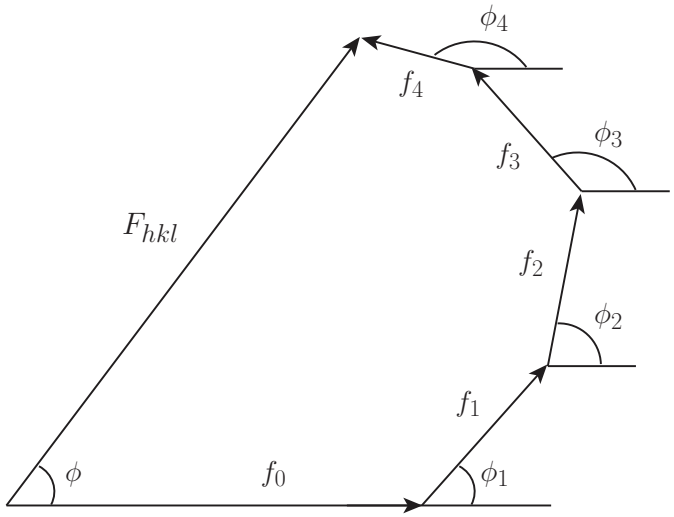

Figure A.2: The atomic form factors which make the angle ϕ_i to the horizontal line are sum as the vector. The structure factor is the result of them.

APPENDIX B

Interstitial site

There are two interstitial sites in the hcp and the fcc phases; the tetrahedral site and the octahedral site. The tetrahedral site is surrounded at the center by four nearest neighbors which form as a tetrahedron. Three spheres at below layer form as the equilateral triangle base and one sphere at above layer is a cap of the tetrahedron. The octahedral site is surrounded at the center by six nearest neighbors which form as a octahedron. Two spheres at below layer and two spheres at above layer form as the square base and another spheres which one at below layer and one at above layer are caps of the octahedron.

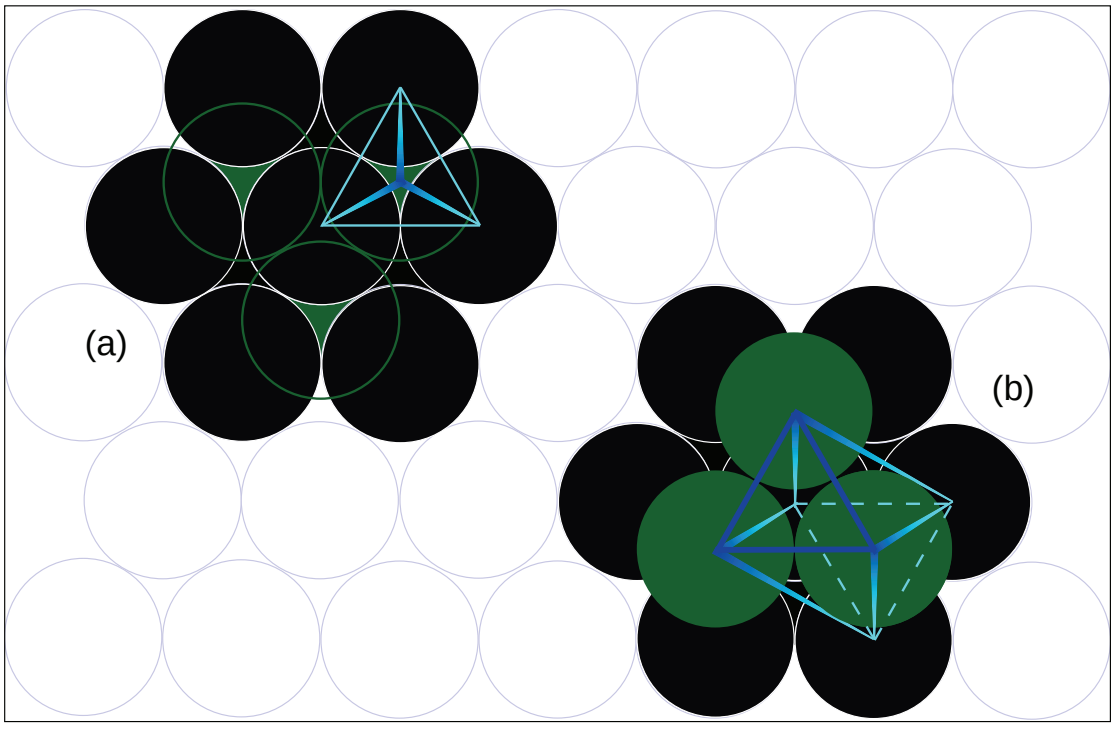

Figure B.1: (a) The tetrahedron is formed by four spheres. (b) The octahedron is formed by six spheres.

APPENDIX C

Exchange-correlation functional

In CASTEP, the enchange-correlation functional for LDA method is separated into two parts; the exchange energy and the correlation energy.

$$E_{xc}[\rho] = E_x[\rho] + E_c[\rho], \tag{C.1}$$

where ρ is the electron density. The exchange energy was modeled by Thomas, Fermi and Dirac [23] which has the form as

$$E_x^{LDA}[\rho] = C_x \int \rho^{4/3}(\mathbf{r}) d\mathbf{r}, \tag{C.2}$$

where $C_x = 0.7386$. The correlation energy was modeled by Ceperley and Alder (CA) [13] which can be written in the form of energy density as

$$\varepsilon_c^{CA} = \frac{A}{2}\Bigg\{ \ln\frac{x}{X(x)} + \frac{2b}{Q}\tan^{-1}\frac{Q}{2x+b} - \frac{bx_0}{X(x_0)}\left[\ln\frac{(x-x_0)^2}{X(x_0)} + \frac{2(b+2x_0)}{Q}\tan^{-1}\frac{Q}{2x+b}\right]\Bigg\}, \tag{C.3}$$

where $x = r_s^{1/2}$, $X(x) = x^2 + bx + c$, $Q = (4c - b^2)^{1/2}$ and r_s is the correlation hole radius with dimensionless. The parameters were parameterized by Perdew and Zunger [14]. The enchange-correlation functional for GGA method is so as for LDA method which is separated into two parts. The exchange energy can be written as

$$E_x^{GGA}[\rho] = \int \rho^{4/3}\varepsilon_x(\rho)F_x(s)d\mathbf{r}. \tag{C.4}$$

The correlation energy is used the PBE (Perdew-Burke-Ernzerhof) model [15] which has the form as

$$E_c^{PBE}[\rho_\uparrow, \rho_\downarrow] = \int \rho[\varepsilon_c(r_s,\zeta) + H(r_s,\zeta,t)]d\mathbf{r}, \tag{C.5}$$

where

$$H = (e^2/a_0)\gamma\phi^3 \times \ln\left\{1 + \frac{\beta}{c_0}t^2\left[\frac{1+At^2}{1+At^2+A^2t^4}\right]\right\}, \tag{C.6}$$

$$A = \frac{\beta}{\gamma}\big[\exp -\varepsilon/(\gamma\phi^3 e^2/a_0) - 1\big]^{-1}, \tag{C.7}$$

$$\zeta = \frac{(\rho_\uparrow - \rho_\downarrow)}{(\rho_\uparrow + \rho_\downarrow)}. \tag{C.8}$$

APPENDIX D

Quasi-Newton method

The quasi-Newton method is one of the optimization method which finds a local maximum or minimum value of the problem. It can find the extremum value by expanding the function $f(x)$ around the x with the Taylor's series

$$f(x_k + \Delta x) \approx f(x_k) + \nabla f(x_k)^T \Delta x + \frac{1}{2} \Delta x^T B \Delta x, \tag{D.1}$$

where B is the Hessian matrix. The optimization process evolves the parameter x_k until the evolved function, $f(x_k + \Delta x)$, reaches the extremum. From Eq D.1, the gradient of the evolved function can be written as

$$\nabla f(x_k + \Delta x) \approx \nabla f(x_k) + B \Delta x, \tag{D.2}$$

At extremum, the gradient of the evolved function will be zero, so

$$\Delta x = -H \nabla f(x_k), \tag{D.3}$$

where H is the inverse of the Hessian matrix, B^{-1}. The evolved parameter, x_{k+1} can be found by the line search method

$$x_{k+1} = x_k + \alpha_k p_k, \tag{D.4}$$

where $p_k = \Delta x$ and α_k is a step length. The inverse Hessian matrix can be evolved by the BFGS (BroydenFletcherGoldfarbShanno) method [19]

$$H_{k+1} = H_k + \frac{(s_k^T y_k + y_k^T H_k y_k)(s_k s_k^T)}{(s_k^T y_k)^2} - \frac{H_k y_k s_k^T + s_k y_k^T H_k}{s_k^T y_k}, \tag{D.5}$$

where $s_k = \alpha_k p_k$ and $y_k = \nabla f(x_{k+1}) - \nabla f(x_k)$. Therefore, the parameter that give the extremum value from the function can be found by following algorithm.

Algorithm

- Guess x_0 as the initial value and set H_0 to be identity matrix, $\mathbf{I}$
- Compute the descent direction $p_k = -H_k \nabla f(x_k)$
- Compute the step length $\varphi(\alpha_k) = f(x_k + \alpha_k p_k)$
- Update $x_{k+1} = x_k + \alpha_k p_k$
- Update H_{k+1} by using BFGS method
- $|\nabla f(x_{k+1})| <$ tolerance value

APPENDIX E

Mulliken population analysis

The plane wave (PW) basis set cannot specify such as atomic charge, bond population, charge transfer etc. directly. It can do through a linear combination of atomic orbital (LCAO) basis set. The quality of projection of the PW basis set onto LCAO basis set is defined by a spilling parameter [24]

$$\mathcal{S} = \frac{1}{N_\alpha} \sum_{\mathbf{k}} w_{\mathbf{k}} \sum_{\alpha} \langle \Psi_\alpha(k) | (1 - \hat{p}(\mathbf{k})) | \Psi_\alpha(\mathbf{k}) \rangle, \tag{E.1}$$

where $|\Psi_\alpha(\mathbf{k})\rangle$ is the PW basis set with its number, N_α, $w_{\mathbf{k}}$ is a weight of a calculated k-point in the Brillouin zone and $\hat{p}(\mathbf{k})$ is a projector operator of Bloch function

$$\hat{p}(\mathbf{k}) = \sum_{\mu} |\phi_\mu(\mathbf{k})\rangle\langle\phi_\mu(\mathbf{k})|, \tag{E.2}$$

where $|\phi_\mu(\mathbf{k})\rangle$ is the LCAO basis set. Therefore, the spilling parameter has the value between 0 to 1. The $\mathcal{S} = 1$ means that the LCAO basis set is orthogonal to the PW basis set. The $\mathcal{S} = 0$ means that the LCAO basis set is perfectly match to the PW basis set. In Mulliken population analysis [25], the charge associated with a given atom A is

$$Q(A) = \sum_{\mathbf{k}} w_{\mathbf{k}} \sum_{\mu}^{onA} \sum_{\nu} P_{\mu\nu}(\mathbf{k}) S_{\mu\nu}(\mathbf{k}), \tag{E.3}$$

where $S_{\mu\nu}(\mathbf{k}) = \langle \phi_\mu(\mathbf{k}) | \phi_\nu(\mathbf{k}) \rangle$ is the overlap matrix and $P_{\mu\nu}(\mathbf{k})$ is the density matrix for the atomic states which can be calculated by

$$P_{\mu\nu}(\mathbf{k}) = \langle \phi^\mu(\mathbf{k}) | \hat{\rho}(\mathbf{k}) | \phi^\nu(\mathbf{k}) \rangle, \tag{E.4}$$

where $\hat{\rho}(\mathbf{k}) = \sum_{\alpha}^{occ} n_\alpha |\chi_\alpha(\mathbf{k})\rangle\langle\chi^\alpha(\mathbf{k})|$ and $|\chi_\alpha(\mathbf{k})\rangle$ is the projected PW state with its occupancy number, n_α. The overlap population between atom A and atom B is

$$n(AB) = \sum_{\mathbf{k}} w_{\mathbf{k}} \sum_{\mu}^{onA} \sum_{\nu}^{onB} 2 P_{\mu\nu}(\mathbf{k}) S_{\mu\nu}(\mathbf{k}). \tag{E.5}$$

There is an interpreting result for the bond population [26, 27]. The high value of the bond population is indicated to the covalent and the low value of the bond population is indicated to ionic bond.

VITAE

Mr. Teerachote Pakornchote was born on 6^{th} September 1988, Bangkok, Thailand. He finished the bachelor degree from Chulalongkorn University in 2011 and continue studying the master degree at the same university. For three years of research, he has the publications as follows,

List of publications:

1. Pakornchote T, Bovornratanaraks T and Pinsook U. Structural phase transition of scandium trihydride under high pressure by using *ab inito*. Siam Physics Congress SPC2013, page 313-316.

2. Pakornchote T, Pinsook U and Bovornratanaraks T. The hcp to fcc transformation path of scandium trihydride under high pressure. **J. Phys. Condens. Matter** 26 (January 2014) : 025405.